NUMERICAL EVALUATION OF THE SEISMIC PERFORMANCE OF EXISTING REINFORCED CONCRETE BUILDINGS WITH CORRODED SMOOTH REBARS

Luigi DI SARNO [1] and Francesco PUGLIESE [2]

[1] Senior Lecturer in Structural Design. Civil Engineering and Industrial Design Department - Institute for Risk and Uncertainty, University of Liverpool, Liverpool, United Kingdom, Luigi.Di-Sarno@liverpool.ac.uk;
[2] PhD Student. Civil Engineering and Industrial Design Department - Institute for Risk and Uncertainty, University of Liverpool, Liverpool, United Kingdom, Francesco.Pugliese@liverpool.ac.uk.

Abstract: Exposure to aggressive environments is one of the most critical problems of reinforced concrete (RC) structures, which can affect both their static and dynamic behaviour. In this paper, the linear and non-linear performance of existing corroded RC framed structures were studied through an advanced numerical model. Moreover, an extensive literature review of models and approaches used for the assessment of RC structures exposed to different levels of corrosion is presented. The numerical evaluation of an existing RC structure subjected to different exposures and degradation was considered. A new approach is presented for the evaluation of the ultimate capacity of RC elements. Such an approach has been compared and validated against a set of the experimental results from the literature. The results of comparative analyses showed that the proposed approach can predict the ultimate capacity of corroded RC components. Linear and Non-Linear analyses were performed using a refined Finite Element (FE) method; the seismic performance evaluated in terms of shear strength degradation, inter-storey displacements, ductility and maximum base shear. The outcomes of the present study demonstrate that corrosion has a significant impact on the structural response of the existing building. Such an effect is a function of the type of exposure. The elastic dynamic analyses of the building have demonstrated that corrosion increases the fundamental periods and, changes the mass participation factor and the mode of vibration, i.e. the external exposure. Nonlinear static analyses showed a significant reduction of the shear capacity and the translation ductility with the increase of the corrosion rate for all lateral loading patterns specified by the Eurocode. The results of the nonlinear dynamic analyses illustrated that the damage and deterioration due to the corrosion attack increased the roof drift-ratio and the inter-storey drift-ratio, as well as a relevant decay of the base shear capacity and early collapse, were noted for high-levels of corrosion. Comparisons between nonlinear static and dynamic analyses were also provided in terms of roof drift-ratios and base shears.

Author Keywords: Corrosion; Corroded RC Components; Structural Modelling; Earthquake Engineering; Corroded Longitudinal Reinforcement; Seismic Performance.

1 INTRODUCTION

The phenomenon of corrosion is one of the leading causes of the deterioration and damage of RC civil infrastructures. Chloride and carbonation attacks cause the increase of the volume of steel rebars and lead to the formation of corrosion products such as rust. As a result, micro-cracks inside the concrete and the concentration of tensile stresses between concrete and steel reinforcements are the main consequences. These induce several types of damage such as the spoiling-off of the concrete cover, the reduction of concrete's compressive strength, the reduced confinement effectiveness of the transverse reinforcements and the bucking of longitudinal rebars (i.e. Di Sarno and Pugliese, 2019 among the others). Despite numerous changes in Standards and Technical Codes over the years, low-strength concrete and inadequate thickness of concrete cover remain prevalent (Bertolini, 2008; Bertolini et al., 2016; Claisse P.A., 2008). Consequently, many RC structures, such as bridges and ordinary buildings, both in non-seismic (Bhide et al., 1999, Di Sarno and Pugliese, 2019) and seismic prone zonas (Biondini et al., 2014; Andisheh et al., 2016; Yalciner et al. 2015), are in poor condition due to ageing. Furthermore, very often inspection-ratings, aimed at assessing the serviceability of a structure, have been inadequate or neglected. Recent studies conducted by Bhide, 1999; Prizl et al., 2014; Radlinska et al., 2014; Arteaga, 2018, found that about 173,000 in the US, that is 10% of the total RC bridges, are structurally deficient and functionally obsolete. Thus, an investment of $2.5 trillion in the US would be needed to restore those "substandard" structures" to suitable condition. In addition, a survey carried out by Ueli M. Angst (2018) estimated that direct costs related to corrosion prevention, control, and repair in the US for RC structures amount to 25 billion dollars. Many experimental campaigns have been conducted on the seismic and non-seismic performance of the structural components exposed to corrosion, such as beams (Azad et al., 2004; Coronelli and Gambarova, 2004; Ye et al., 2018; Cairns et al., 2008; Khan et al., 2012; Rodriguez et al., 1997; Torres-Acosta et al., 2007; Xia et al., 2011; Val et al., 2009), columns (Revathy et al., 2009; Rodriguez et al., 1996; Shi et al., 2001; Wang and Liang, 2008), and steel reinforcements (Andrade et al., 1991; Cairns et al., 2005; Clark et al., 1994; Du et al., 2001; Imperatore et al., 2017; Lee et al., 1996; Morinaga, 1996; Wang and Liu, 2008). Some research focused on the performance of the entire RC structures exposed to corrosion (Biondini et al., 2011; Celarec et al., 2011; Di Sarno and Pugliese, 2019; Pugliese et al., 2019; Yalcimer et al., 2015; Zhang et al., 2018;). Khank et al. (2012) presented an interesting study on 26-year old RC beams exposed to natural corrosion to assess their performance after long-term damage. The 26-year old beams were then tested until they failed, and the force-displacement curves were obtained. Results showed a significant reduction of the load-bearing capacity, the stiffness and the deflection of the beams. Coronelli and Gambarova (2014) conducted a numerical study on RC beams exposed to corrosion. They used a non-linear finite approach to predict the capacity of RC beams. Significant stiffness decay, strength deterioration in bending and shear, and bond failure are the main results of this numerical study. Rodriguez et al. (1997) conducted an experimental campaign to evaluate the load-bearing capacity of corroded RC columns using three different configurations for steel reinforcements. They found that corrosion negatively affects the performance of the RC columns. In fact, it reduces the load-bearing capacity and the ultimate strains, and damages the concrete cover, and as a result it causes a premature buckling of rebars. Furthermore, axial loading eccentricity increased with high levels of corrosion. Xia and al. (2015) presented an experimental investigation on the performance of RC columns when steel reinforcements are exposed to different levels of corrosion. Corrosion was simulated via the use of the combined electrochemical process and wet-dry-cycles, while columns were subjected to eccentric compressive loading. Cracking patterns and load-bearing capacity were the focus of this study. They found that corrosion induced large cracks, especially for high corrosion rate levels, while large eccentricity and small stirrups reduced the compressive bearing capacity of the columns, whereas the corroded rebars led to cover cracking, spalling and delamination. Vu and Li (2018) carried out an experimental study on eight-full scale un-corroded and corroded RC columns to investigate the impact of corrosion on the seismic performance of these short columns that failed in shear. Drift capacity, hysteretic response and deformation capacity were the parameters evaluated in this study. They found that shear strength and deformation capacity significantly decreased with the increase of the corrosion rate, especially when columns were subjected to highly corrosive environments and high axial-load ratios. Meda et al. (2014) conducted an experimental campaign to evaluate the behaviour of corroded RC columns under cycling loading to simulate earthquake excitations. Preliminarily, they performed some tests on rebars to investigate the corrosion effects on their mechanical properties for different levels of corrosion. Full-scale RC columns under a simulated seismic load were used for this study. The results showed a decrease of 30% in base shear and 50% in the drift capacity. Yalciner et al. (2015) conducted a study to analyze the behaviour of a 50-year old school building considering the effects of corrosion over the years. Non-linear static and incremental dynamic analyses were performed on a two storey-frame to predict the time-dependent performance level of the structure. They considered two corrosion effect parameters, i.e. bond-slip and reduction of steel reinforcement cross-sectional area. The most relevant evidence of this study was that the bond strength of the two-storey frame decreased as the corrosion increased. Karapetrou et al. (2017) carried out a study on the assessment of the seismic vulnerability of RC structures considering the ageing effects over time. Their Incremental Dynamic analyses (IDA) showed the increase of the overall seismic vulnerability in correspondence to increased levels of corrosion. Zhang et al. (2018) performed a numerical evaluation of the seismic performance of a six-storey-three span RC frame considering different levels of corrosion. The degradation parameters were analyzed using non-linear static analyses. Results clearly showed a relevant decrease of the seismic performance of the RC frame and a significant increase of the inter-storey drift ratio.

All these studies showed a critical reduction of the load-bearing capacity, shear strength and ductility of RC structures, which became more critical when the buildings were subjected to seismic loadings. Particularly, corrosion can be extremely relevant in seismic prone areas if stirrups spacing does not provide enough lateral confinement to withstand seismic loadings, which can change the global behaviour of RC buildings. However, the experimental research about the effect of corrosion on the seismic performance of RC structures is still minimal and additional studies are needed to obtain a full understanding of their 3D behaviour. Although 2D studies may give a relevant indication of the behaviour of RC frames, they do not consider the interaction and redistribution of actions between frames. This paper presents a novel approach to evaluate and assess the ultimate capacity of RC components exposed to different levels of corrosion. The proposed method will help to overcome excessively conservative repair solutions and, at the same time, preserve the safety of RC structures, both in seismic and non-seismic areas. A case study representing protected RC structures is presented and investigated via a Finite element approach, which consists of Force-Based element frames and fiber sections accounting for the modified stress-strain constitutive models of the concrete and steel rebars. Push-over, spectrum-compatibility and time-history analyses with respect to the European Limit States (Eurocode 8, Part-3) are performed to assess the performance of the existing RC structure when exposed to different levels of corrosion by means of the shear strength, ductility and inter-storey displacements. The results showed a critical reduction in both base shear and ductility, as well as an alteration of the failure mode when exposed to high levels of corrosion. Moreover, a significant increase of the inter-storey displacements was noted, and, therefore, an earlier collapse of the corroded RC structure when time-history analyses were performed. It is worth noting that the above-mentioned study was one of the very few that considered full-scale corroded RC structures. So, the present contribution may help to provide a better understanding of the seismic vulnerability of RC structures subjected to aggressive environments and high levels of corrosion.

2 RESEARCH SIGNIFICANCE

This study aims at investigating the ultimate capacity of RC components and the seismic performance of existing RC buildings with corroded steel reinforcements considering different type of exposure, i.e. only columns, only beams, both beams and columns and a real external exposure. A numerical approach is provided to assess the ultimate capacity of both RC members under axial loads and corroded RC columns under simulated cycling loads. A set of experimental tests were used to validate the proposed numerical approach. The present study also includes the evaluation and simulation of the seismic response of an existing RC structure by nonlinear Static and Dynamic analyses using revised performance criteria for corroded RC components. Pushover analyses were carried out by using three different lateral loading patterns and compared to, in terms of shear and deformation capacity, nonlinear dynamic analyses. A study for the impact of corrosion on the q-factor, the overstrength and ductility is also carried out. Significant effort was made to perform nonlinear dynamic analyses for the specified Limit States to provide the behaviour of the RC building when exposed to different levels of corrosion and subjected to various ground motion intensities. This study can be useful for establishing new-inspection ratings for corroded RC structures to mitigate the risk and reduce conservative repair-solutions.

3 MECHANICAL PROPERTIES OF CONCRETE EXPOSED TO CORROSION

Several projects and theoretical studies have been conducted on the behaviour of concrete when exposed to different levels of corrosion (Asborra et al. 2010; Khan et al., 2014; Shayanfar et al., 2016; Zandi et al., 2011). Both carbonation and chloride-induced corrosion are the main causes of concrete degradation. Potentially, these two chemical processes can lead to cracking in the concrete cover and the successive spoiling-off, and cracking in the concrete core due to the expansion of the corrosion products. Besides, the increase in the volume of the rust affects the local stresses between the concrete and rebars which causes the loss of bond. However, the effect of corrosion does not only affect the compressive strength of the concrete cover, but the spoiling-off exposes the stirrups, which are effective for withstanding shear forces, to corrosion by reducing the load and the deformation capacity of RC members during an earthquake. Although many studies have been carried out, it is still challenging to use an analytical method to determine the reduction and the location of the deterioration. Coronelli and Gambarova (2014) proposed a method to account for the impact of corrosion on the concrete's compressive strength based on the numerical evaluation of corroded RC beams and the Vecchio and Collins'study (1992). They provided a relationship to simplify the impact of corrosion on the reduction of the concrete's compressive strength, as follows:

$$\beta_c = \frac{f_c^*}{f_c} = \frac{1}{1 + K\frac{2\pi X n_{bars}}{b\varepsilon_{c2}}} \tag{1}$$

where f_c^* represents the corroded compressive strength, f_c the uncorroded compressive strength, K a constant equal to 0.1 for medium rebar, X the corrosion penetration, b the width of the cross-section, ε_{c2} strain at the peak and n_{bars} the number of steel reinforcement in the compressive zone. In the relationship (1), n_{bars} represents the number of reinforcements in the top layer (compressive zone) and f_c^* applied on the entire section. However, the reduction of the concrete's compressive strength should be only considered on the side of the attack and applied only on the effective area exposed to corrosion; otherwise, the reduction will be excessively high and the ultimate capacity underestimated.

4 MECHANICAL PROPERTIES OF CORRODED STEEL REINFORCEMENT

The degradation due to corrosion of the steel reinforcements embedded into the concrete is among the main concerns while assessing RC components and structures with ageing. When corrosion occurs, the penetration can be measured on-site by using the following formulation:

$$x(t) = \int_{t_i}^{ti+t_p} r_{corr}\, dt \tag{2}$$

where r_{corr} (mm/year) is the steel corrosion rate, t_p represents the propagation time and t_i the initiation time (it does not correspond to zero). Figure 1 describes the typical time of corrosion initiation and propagation (Tuuti, 1982). The reduction of the cross-section of the rebar can be calculated through a coefficient γ that ranges between 0 and 1, as follows:

$$\gamma = \frac{x(t)}{\varphi_0} \tag{3}$$

where $x(t)$ is the corrosion penetration in mm and φ_0 is the initial diameter of the steel reinforcement.

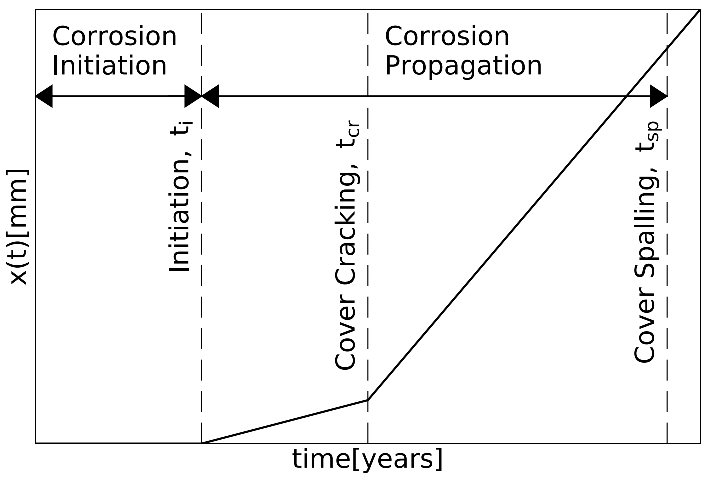

Figure 1. Corrosion Initiation and Propagation (Tuutti, 1982)

However, the definition of the corrosion penetration, and therefore the coefficient γ depends on the type of corrosion, which can be either uniform or localized. If corrosion is a result of concrete carbonation, the attack is more likely to be uniform along the bar (Uniform Corrosion), while if corrosion is due to chloride contents, the attack is more likely to be localized at some points along the bar (Pitting Corrosion). The carbonation and low-chloride contents lead to a steady reduction of the mechanical properties of the steel reinforcements, while the high-chloride contents cause a worse localized decay of the above-mentioned steel properties, such as strength and ductility (Biondini et al., 2012).

4.1 YIELDING STRESS REDUCTION

Many experimental tests have been conducted to investigate the impact of corrosion on the mechanical properties of steel reinforcements, both embedded and bare bars. Mostly, these experimental campaigns were carried out on deformed steel reinforcements. According to these experimental tests, a relationship between the mass loss due to corrosion and the yield stress reduction can be derived. The general equation can be expressed as follows:

$$f_y^* = (1 - \beta_S CR[\%]) f_y \tag{4}$$

where f_y^* is the corroded yielding stress, f_y the un-corroded yielding stress, β_S the experimental coefficient and $CR[\%] = \frac{M_0 - M_C}{M_0}$ the mass loss based on the mass before (M_0) and after corrosion (M_C). Table 1 provides a comprehensive indication of some experimental campaigns conducted over the years.

Table 1. Empirical Coefficients for reduced steel yielding stress

Reference	Type	Exposure	CR [%]	β_S
Du et al. (2001)	Bare Rebar	Accelerated	0-25	0.0140
Du et al. (2001)	Embedded Rebar	Accelerated	0-18	0.0150
Morinaga et al. (1996)	Embedded Rebar	Service-Chlorides	0-25	0.0170
Zhang et al. (1995)	Embedded Rebar	Service-Carbonation	0-67	0.0100
Andrade et al. (1991)	Bare rebar	Accelerated	0-11	0.0150
Clark et al. (1994)	Embedded Rebar	Accelerated	0-28	0.0130
Lee et al. (1996)	Embedded Rebar	Accelerated	0-25	0.0120
Cairns et al. (2005)	Embedded Rebar	Accelerated	0-3	0.0120
Du et al. (2005)	Embedded Rebar	Accelerated	0-18	0.0050
Andisheh et al. (2016)	Theoretical Study	Accelerated/Natural	0-80	0.0198
Wang and Liu (2008)	Embedded Rebar	Accelerated	0-10	**
Imperatore et al. (2017)	Both	Accelerated	0-40	**

*** The value is different depending on whether it is uniform or pitting corrosion as it is explained in Table 2*

These empirical coefficients are mostly referred to one type of corrosion and, in many cases, uniform and localized corrosion are combined. Instead, Wang et al., 2008 and Imperatore et al., 2017 provided empirical coefficients for both uniform and pitting corrosion, which make these studies more reliable and accurate in comparison with the results from the literature. Furthermore, the latter studies demonstrated an excellent Parson's coefficient factor, which is the measure of the linear correlation between two variables and it is almost one in the Imperatore and Wang's studies as shown in Table 2.

Table 2. The correlation coefficient for uniform and localised corrosion

Reference	Type of Corrosion	β	Correlation Factor
Wang and Liu (2008)	Uniform	0.0124	0.7800
	Pitting	0.0198	0.9200
Imperatore et al. (2017)	Uniform	0.0151	0.9263
	Pitting	0.0199	0.9234

In this study, the relationships given by Imperatore et al. (2017) were used as they included many experimental tests from the literature and, particularly, were more consistent with the phenomenon of the corrosion of steel reinforcements. Figure 2 shows the relationship between the reduced steel yielding stress and the corrosion rate:

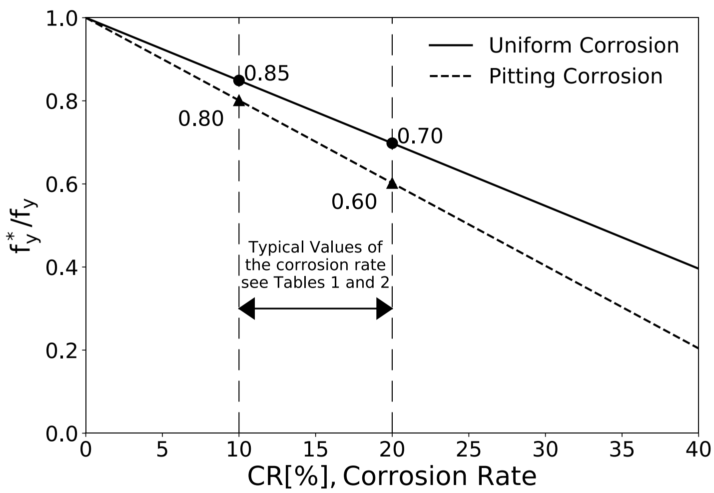

Figure 2. Steel Yielding Stress vs Corrosion Rate

The typical values of corrosion (10%-20%) for existing RC structures after a lifetime of roughly 20 years is given in Figure 2. The reduction of the yielding stress depends on the type of corrosion and, ranges from 15% to 30% for uniform corrosion and from 20% to 40% for pitting corrosion.

4.2 ULTIMATE STRAIN

Experimental tests have demonstrated that low and high levels of corrosion reduced significantly the ductility of the steel rebars (Kobayahi et al., 2006; Coronelli and Gambarova, 2004; Apostopoulos et al., 2008; Biondini et al., 2011; Imperatore et al., 2017). According to these experimental tests, the behaviour of the steel reinforcements and, therefore, the RC elements may shift the failure mode from ductile to brittle, especially for high levels of corrosion. Kobayashi (2006) proposed a relationship for the residual ultimate strain of the steel reinforcements when exposed to corrosion based on experimental results:

$$\frac{\varepsilon_{su}^{*}}{\varepsilon_{su}}[\%] = 100 - 18.1x[\%] \tag{5}$$

where x represents the cross-sectional reduction. Yet, the relationship referred to experimental tests with low levels of corrosion, so it becomes useful for a mass loss between 3% and 5%. Coronelli and Gambarova (2004) proposed a relationship accounting also for the pitting:

$$\varepsilon_{su}^{*} = \varepsilon_{sy} + (\varepsilon_{su} - \varepsilon_{sy})\left(1 - \frac{\alpha_{pit}}{\alpha_{pit,max}}\right) \tag{6}$$

where ε_{sy} is the steel strain at yielding, α_{pit} and $\alpha_{pit,max}$ are respectively the depth and maximum depth of the pitting attack. The coefficients of pitting corrosion are difficult to determine because they require consistent on-site study of existing RC structures. Biondini et al. (2011), based on the experimental campaign conducted by Apostopoulos et al. (2008), provided a relationship for the ultimate strain of corroded steel rebars:

$$\varepsilon_{su}^{*} = \begin{cases} \varepsilon_{su} & 0 \leq CR[\%] \leq 1.16 \\ 0.1521\, CR^{-0.4583}\varepsilon_{su} & 1.6 \leq CR[\%] \leq 100 \end{cases} \tag{7}$$

However, the formulation (7) is based on a single experimental campaign and does not consider other types of corroded steel reinforcements. Imperatore et al. (2017) carried out an extensive experimental campaign, which also included results from the literature. They provided relationships both for uniform and localized corrosion, as follows:

$$\begin{cases} \varepsilon_{su,pitting}^{*} & = \varepsilon_{su} e^{-0.0547CR[\%]} \\ \varepsilon_{su,uniform}^{*} & = \varepsilon_{su} e^{-0.0277CR[\%]} \end{cases} \tag{8}$$

These experimental results have demonstrated that the corrosion does not affect the elasticity modulus of the steel rebars. Figure 3 illustrates the ultimate strain with the increase of corrosion rate both for uniform and localized corrosion, and the typical values of corrosion (10%-20%) for an existing RC structure:

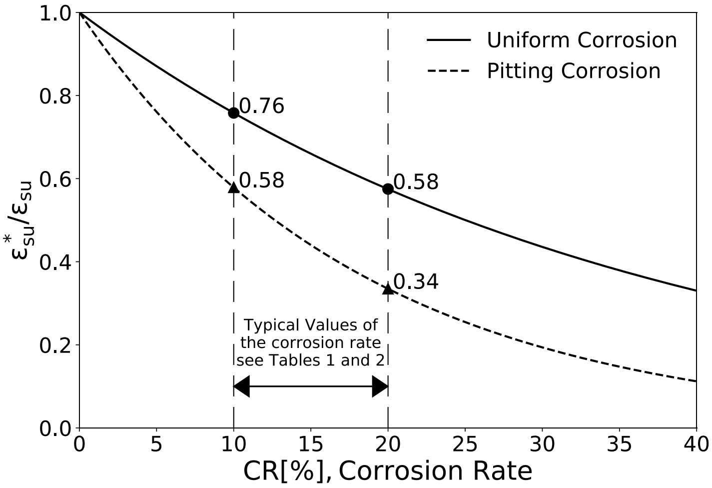

Figure 3. Ultimate Strain of corroded steel reinforcement

Figure 4 illustrates the bilinear stress-strain model of corroded steel reinforcement which exploits the equations (4) and (8):

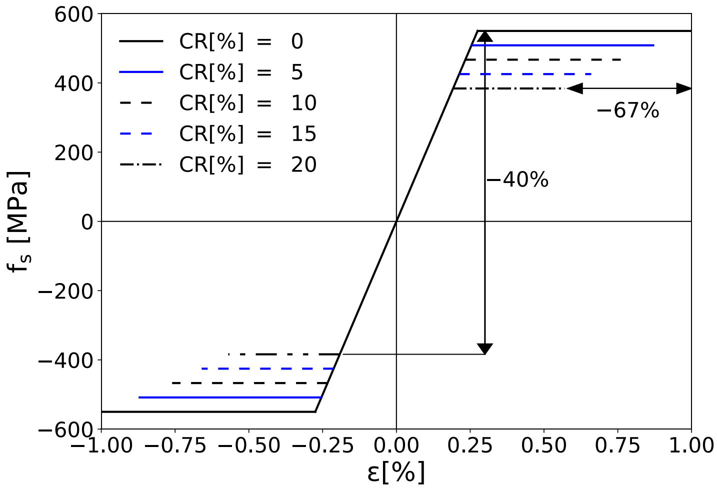

Figure 4. Bilinear Stress-Strain model for corroded Steel reinforcement

Corrosion reduces significantly the yielding stress and the ultimate strain of steel reinforcements by 40% and 67% respectively with the increase of the corrosion rate up to 20%.

5 VALIDATION OF THE PROPOSED NUMERICAL MODEL

5.1 MODEL CALIBRATION

A new method for the evaluation of the ultimate capacity of RC members was proposed by Di Sarno and Pugliese (2019), which consists in dividing the RC cross-section into three concrete blocks containing the concrete cover, the un-effective confined core and the effective enclosed core. The concrete cover represents the clear cover (CC) until the transverse reinforcement, while the un-effective (UCC) and effective (ECC) confined concrete are respectively the area twice the diameter of longitudinal reinforcement bars and the remaining uncorroded area of the concrete (Figure 5). Once corrosion occurs, only the compressive strength of the concrete cover and un-effective confined concrete will be reduced by the use of the coefficients β_C in Eq. (1). The reason for the different concrete blocks is to simulate the real behaviour of RC members. Accordingly:

$$f_c^* = \frac{\beta_C f_c A_{CC} + \beta_C f_{cc} A_{UCC} + f_{cc} A_{ECC}}{A_{CC} + A_{UCC} + A_{ECC}} \tag{9}$$

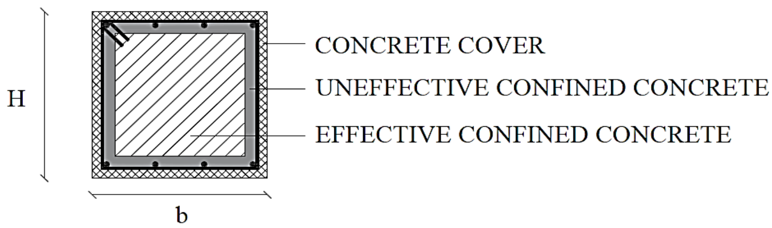

Figure 5. Concrete blocks

Figure 6 shows a comparison between the two methods (Coronelli and Gambarova, 2008; Di Sarno and Pugliese, 2019) in terms of the reduction in the concrete's compressive strength with the increase of the corrosion penetration based on the experimental results conducted by Rodriguez et al., 1996.

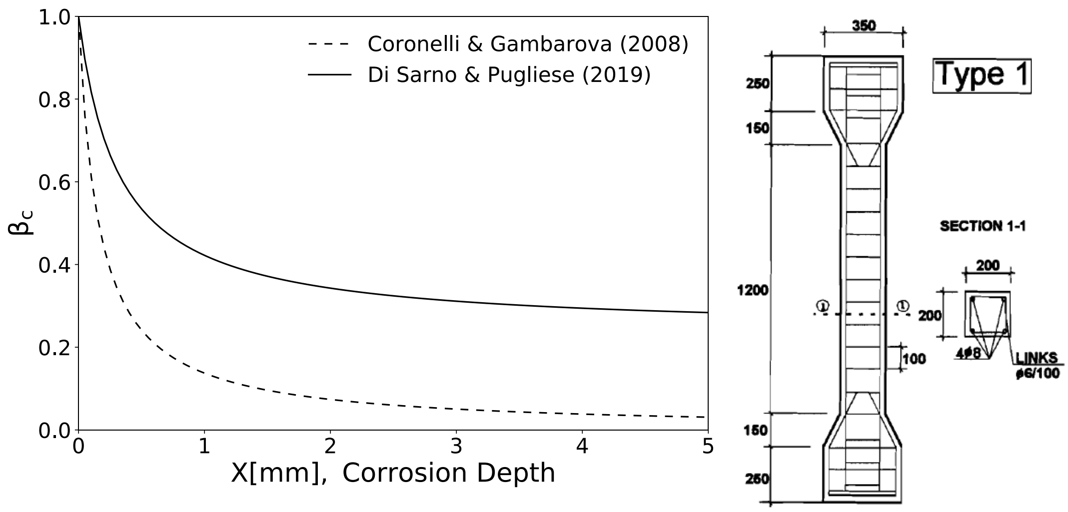

Figure 6. Concrete compressive strength reduction (after Rodriguez et al., 1996; Type 1)

Despite numerous experimental tests on the behaviour of corroded concrete, no results are available from the literature on the strain at the peak of the compressive strength and the ultimate strain when the concrete is exposed to different levels of corrosion. As a result, the latter parameters were reduced according to the compressive strength. To simplify the calculation for the mass loss, Zhang et al.

(2018) proposed a relationship between the corrosion loss ratio of the rebar section ρ_s, the radius of the steel rebars r and the mass-loss rate of the corroded steel δ, as follows:

$$\rho_s = \frac{2X}{r} - \left(\frac{X}{r}\right)^2 \tag{10}$$

$$\rho_s = \begin{cases} 0.013 + 0.987\delta & \delta \leq 10\% \\ 0.061 + 0.969\delta, & 10\% < \delta \leq 20\% \\ 0.129 + 0.871\delta, & 20\% < \delta \leq 30\% \\ 0.199 + 0.810\delta, & 30\% < \delta \leq 40\% \end{cases} \tag{11}$$

According to Eurocode 2 Part 1-1 (EN-2, 2005), the stress-strain relation of concrete will be approximated by a parabola-rectangle diagram, which is convenient to use in analytical studies as it is continuous up to the strain at maximum strength and flat until the ultimate strain:

$$f = \begin{cases} f_c\left[1 - \left(1 - \frac{\varepsilon_c}{\varepsilon_{c2}}\right)^n\right] & 0 \leq \varepsilon_c \leq \varepsilon_{c2} \\ f_c & \varepsilon_{c2} \leq \varepsilon_c \leq \varepsilon_{cu} \end{cases} \tag{12}$$

where:

$$n = \begin{cases} 2.0 & 0\,MPa \leq f_c \leq 50MPa \\ 1.4 + 23.4\left(\frac{90 - f_c}{100}\right)^4 & 50MPa \leq f_c \leq 90MPa \end{cases} \tag{13}$$

$$\varepsilon_{c2}[‰] = \begin{cases} 2.0 & 0\,Mpa \leq f_c \leq 50MPa \\ 2.0 + 0.085(f_c - 50)^{0.53} & 50MPa \leq f_c \leq 90MPa \end{cases} \tag{14}$$

$$\varepsilon_{cu}[‰] = \begin{cases} 3.5 & 0\,Mpa \leq f_c \leq 50MPa \\ 2.6 + 35\left(\frac{90 - f_c}{100}\right)^4 & 50MPa \leq f_c \leq 90MPa \end{cases} \tag{15}$$

Figure 8 illustrates the comparison of the two models (Coronelli and Gambarova, 2004; Di Sarno and Pugliese, 2019) for the stress-strain of the corroded concrete model by using the specimen Type 1 of Rodriguez et al. (1996) with a penetration attack X of 0.32 mm.

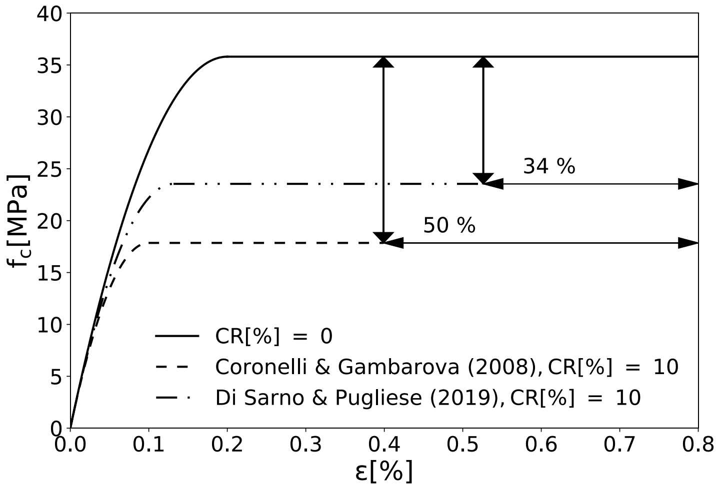

Figure 7. Stress-Strain Models for the corroded concrete

As shown in Figure 7, corrosion affects the two main properties of plain concrete, such as the ductility and the strength. The method proposed by Coronelli and Gambarova (2004) leads to a reduction of the strength and the ductility by 50%, while the method provided by Di Sarno and Pugliese (2019) decreased the previously mentioned mechanical properties by 34%. Moreover, a comprehensive experimental campaign is being carried out by Di Sarno and Pugliese (2019) to evaluate the reliability of the formulation.

Since the proposed method by Di Sarno and Pugliese (2019) deals also with the confined concrete, a comprehensive literature review was carried out to account for the confined ultimate compressive strain for the concrete. It is well-known that the effectiveness of the confinement in concrete is relevant to prevent shear failure during a seismic event. In the design of RC structures, it often refers to an ultimate strain of 0.35% which is too conservative and too far away for predicting the real deformation capacity of RC members. Thus, the method proposed by Razvi et al. (1992) is herein used. They provided a mathematical model to express the stress-strain of concrete confined by transverse reinforcements based on a series of experimental tests carried out on 170 full-size confined concrete columns and including many experimental tests from the literature. It incorporated the most relevant parameters observed for confinement over the years such as the volumetric ratio, spacing, yielding strength and arrangement of transverse reinforcement as well as it covered a wide range of concrete strength, from 30 to 130 MPa, and geometry sections. The proposed numerical method was compared with the experimental results showing an excellent accuracy in predicting the ultimate compressive strain. Here, the relationships:

$$\varepsilon_{ccu} = 5.33\varepsilon_{85} - 4.33\varepsilon_{cc} \tag{16}$$

$$\varepsilon_{85}, \varepsilon_{cc} = f\ (f_{cc}, f_l, \rho_c, s, d_s, f_y) \tag{17}$$

ε_{85} is the strain at the 85% of the confined compressive strength $0.85f_{cc}$; ε_{cc} is the strain at the peak of the confined compressive strength f_{cc}; f_l lateral pressure; s stirrups spacing; ρ_c total transverse steel area in two orthogonal directions divided by corresponding concrete area; d_s stirrup diameter; f_y yielding stress.

5.2 INTERACTION SURFACE

The assessment of the ultimate capacity of RC elements was carried out by the Interaction Surface M-N, which can be used as a reliable tool both in the design and the verification of RC components (Figure 8)

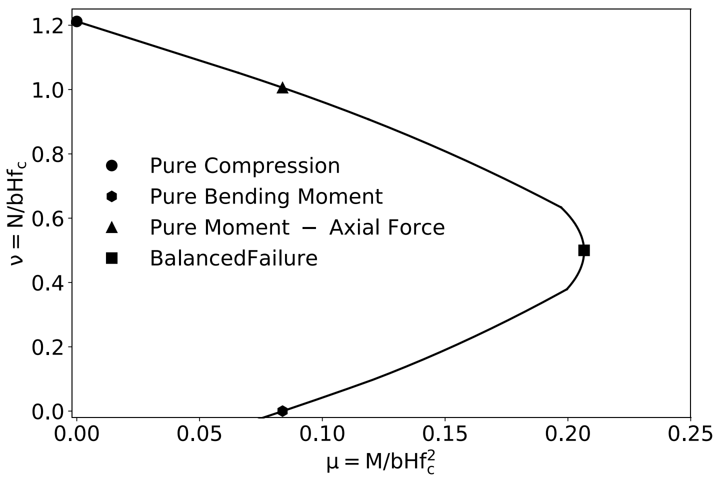

Figure 8. Generic Interaction Domain M-N

The ultimate compressive strains for concrete and steel are set at the values from (16) and 1% respectively. Based on the strain distributions, the stresses and the location of the neutral axis are determined. Experimental results carried out by Rodriguez et al. (1996) were used to validate the proposed method. The tested columns were poured with an additional solution of Calcium Chloride to target the accelerated corrosion, while the impressed current was used to corrode the samples. An incremental axial displacement was applied to the column to reach failure. The results of the numerical simulations are given in Figure 9 and Figure 10:

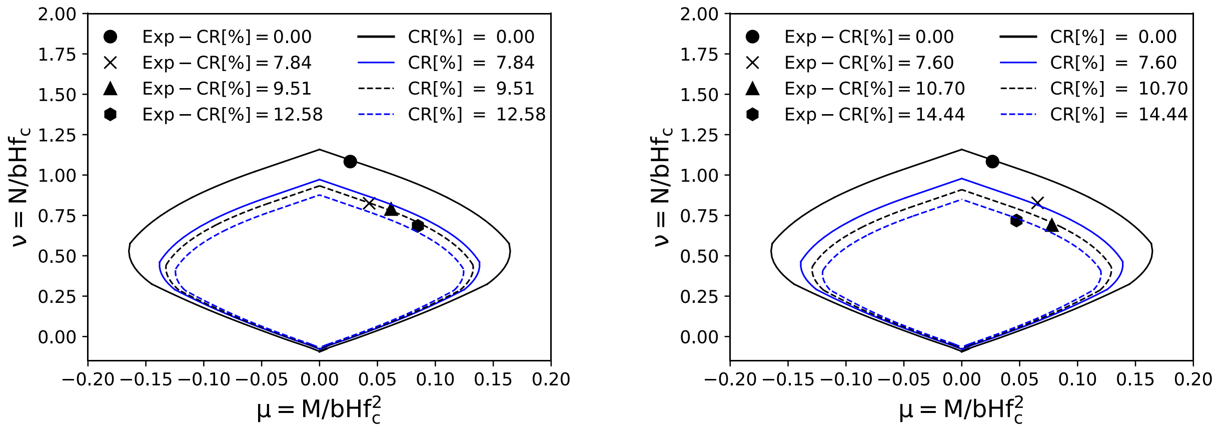

Figure 9.Numerical Validation of the column Type 1 Rodriguez et al. 2006, $\rho_s = 0.5\%$

The results of the proposed method show an excellent agreement with the experimental results for RC columns exposed to corrosion (the points in Figure 9 and 10 represent the ultimate capacity of the tested RC columns), even for different geometrical reinforcement ratios.

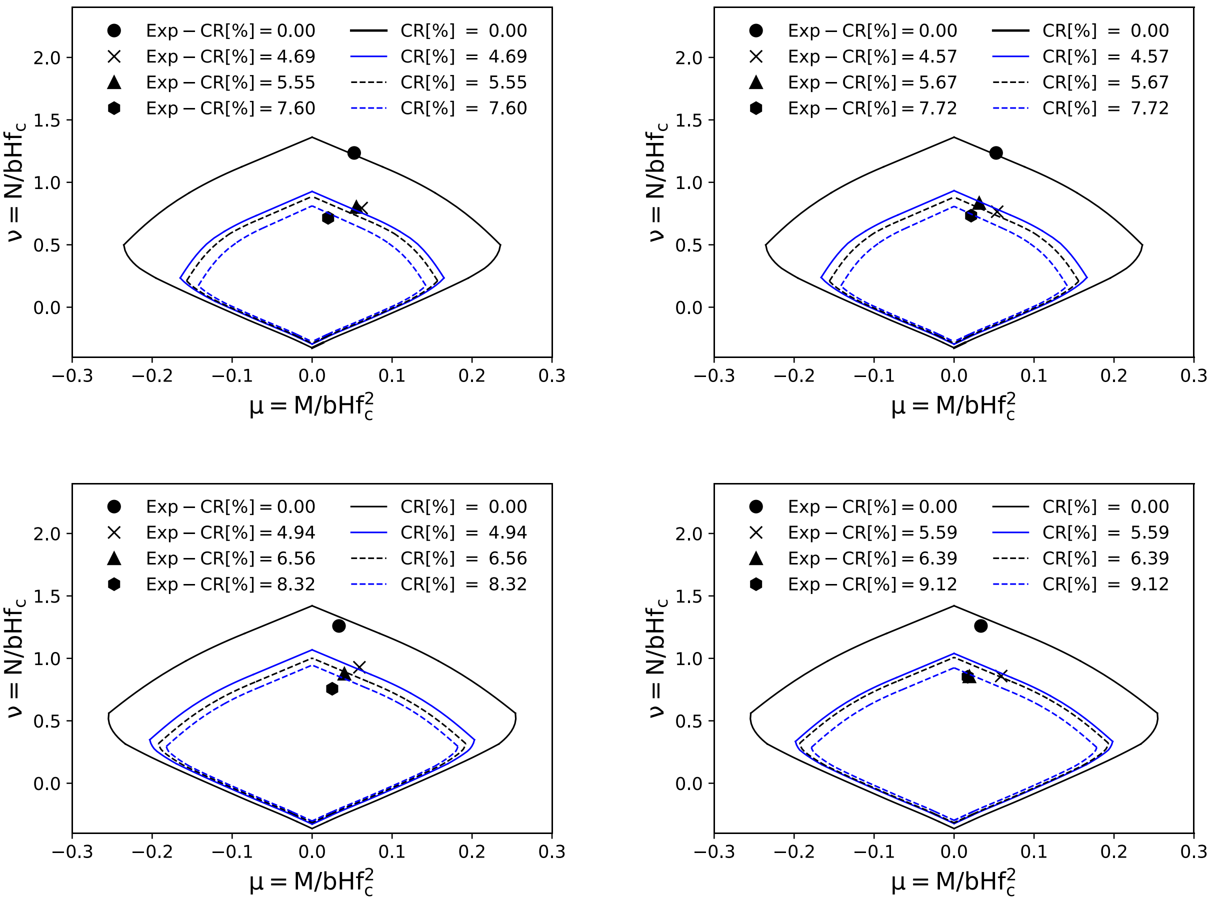

Figure 10. Numerical Validation of the column. a) and b) Type 2 [Rodriguez et al. (2006)], $\rho_s = 2.01\%$; c) and d) Type 3, $\rho_s = 2.26\%$

5.2 CORRODED RC COLUMNS UNDER MONOTONIC LOADING

Numerical validation was also carried out using both the un-corroded and the corroded RC columns under cycling loading tested by Meda et al. (2014), which represents a typical column of an RC structure built in Italy in 1960. The column had a cross-section of 300 x 300 mm^2 with concrete compressive strength of 20 MPa and four Φ16 mm longitudinal ribbed steel reinforcements with yielding stress of 521 MPa and hardening ratio of 0.005. The transverse reinforcements consist of Φ8 mm stirrups with a 300mm spacing. One of the columns was uncorroded and used as a reference, while the second RC column was corroded (longitudinal reinforcements) up to a rate of 20%. The results were shown in the load-drift ratio plot both for the un-corroded and corroded column. A Finite Element approach and the software Seismostruct (2018) were used to implement the RC columns. The stress-strain model of Chang and Mander (1992) for concrete was used as suggested in Pugliese and Di Sarno (2019). This concrete model is able to simulate the behaviour both core and concrete cover by modifying the peak strain and the compressive strength as the shape of the constitutive model remains the same. The steel rebars were modelled by using the constitutive model of Monti-

Nuti (1992) with the mechanical properties provided by Meda et al. (2014). Hence, concrete and steel models were modified exploiting the relationships given by Di Sarno and Pugliese (2019) and Imperatore et al. (2017) respectively. Finally, monotonic positive and negative pushover analyses were performed, and the outcomes were validated against experimental results (Figure 11a & Figure 11b).

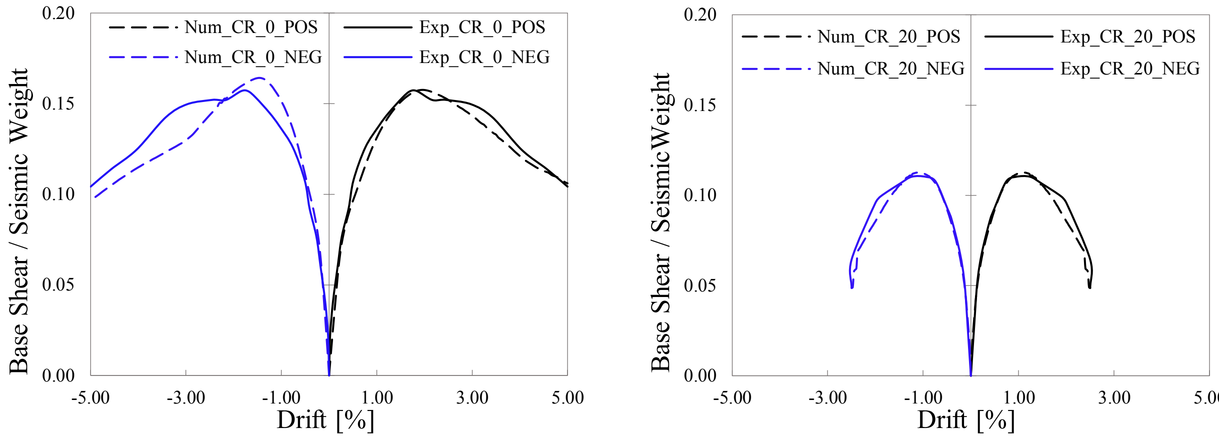

Figure 11. a) Monotonic Positive-Negative Pushover: a) Uncorroded Column; b) Corroded Column

The Base Shear-Drift diagram summarizes the results of the monotonic behaviour of both RC columns. As shown in Figures 11a and 11b, the proposed model is able to predict with excellent accuracy the response of the corroded RC column exposed to a monotonic loading with a negligible error margin of the shear strength and ductility. The maximum values of the base shear obtained from the proposed numerical approach for the un-corroded and corroded column were 65 MPa and 45 MPa respectively, which are close to the values obtained from the experimental tests 63Mpa and 44 MPa. In terms of ductility, the numerical evaluation seems to be in accordance with the experimental results.

6 CASE-STUDY BUILDING

An existing four-storey RC building (SeismoSoft Sample Models, 2018) was considered as a testbed for this study. The building is situated near the sea in San Benedetto del Tronto (Italy). Typical columns with a square-cross-section 350x350 mm^2 and 300x300 mm^2 were used for the ground floor and the other floors respectively, both with 6 smooth longitudinal rebars Φ16mm and transverse stirrups Φ6mm with 150mm spacing. The beams had different cross-sections and the longitudinal reinforcements mostly consisted of Φ14 mm and Φ10 mm diameters. The concrete's compressive strength was 16.73 MPa both for columns and beam, while the steel reinforcement had yielding stress of 440 MPa. The slabs were implemented through rigid-diaphragms as to ensure in-plane stiffness properties, and exhibited neither membrane deformation nor report the associated forces, while all the joints were connected through fully-supported-rigid-connections (all degrees of freedom were restrained) to the ground. An accurate loading analysis was conducted and applied for the beams (loading-range [6.51 kN/m; 10.42 kN/m]).

Table 3. Type of Exposure (COR = corroded; UNC = un-corroded)

CASE STUDY	COLUMNS		BEAMS	
	INTERNAL	EXTERNAL	INTERNAL	EXTERNAL
1	COR	COR	UNC	UNC
2	UNC	UNC	COR	COR
3	COR	COR	COR	COR
4	UNC	COR	UNC	COR

The model of the ordinary RC structures is given in Figure 12a and Figure 12b. Corrosion has been applied to only columns, only beams, the entire building and, on columns and beams externally (see Table 3). Potentially, this procedure allows for the evaluation of the impact of corrosion on different RC elements. Non-linear static and dynamic analyses have been conducted. Both non-linear analyses comply with Eurocode 8-Part 3 (EN-8, 2005).

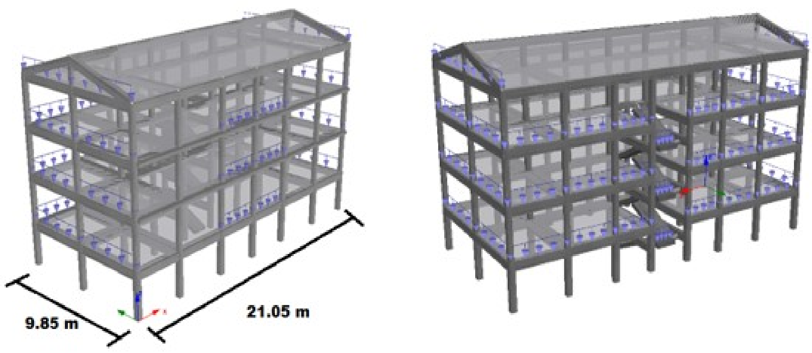

Figure 12. Finite Model of the sample Structure implemented in SeismoStruct: a) North and b) South Views

7 SEISMIC PERFORMANCE ASSESSMENT

7.1 PERFORMANCE CRITERIA

Performance levels can be obtained in the various stage during the pushover analysis and expressed by the normalized base shear and roof displacement. Since no clear standards and limit states for corroded RC structures are available from the literature, different parameters are herein used for defining and evaluating the seismic performance of the existing building according to the Eurocode 8 – Part 3 (EN 1998-3, 2004) and modifications proposed by the authors. The Limit States (LSs) were divided into two categories: global parameters defined in terms of Drift limits according to Eurocode

(EN 1998-1, 2004) with additional provisions (FEMA 356, 2000), and local parameters, both defined in Table 4:

Table 4. Performance criteria

LOCAL PARAMETERS		
DL	**SD**	**NC**
ε_C , θ_C , ε_{SY} , $M_{Y,BMs}$ $\left(N_{Y,COLs}, M_{Y,COLs}\right)$, V_Y	$\varepsilon_{CU,COVER}$, $\frac{3}{4}\theta_U$, $\frac{3}{8}\varepsilon_{SU}$, $M_{U,BMs}\left(\varepsilon_{CU,COVER}, \frac{3}{8}\varepsilon_{SU}\right)$ $\begin{pmatrix} N_{Y,COLs}\left(\varepsilon_{CU,COVER}, \frac{3}{8}\varepsilon_{SU}\right), \\ M_{Y,COLs}\left(\varepsilon_{CU,COVER}, \frac{3}{8}\varepsilon_{SU}\right) \end{pmatrix}$, V_{SD}	$\varepsilon_{CU,CONFINED}$, θ_U , ε_{SU} , $M_{U,BMs}\left(\varepsilon_{CU,CONFINED}, \varepsilon_{SU}\right)$ $\begin{pmatrix} N_{Y,COLs}\left(\varepsilon_{CU,CONFINED}, \varepsilon_{SU}\right), \\ M_{Y,COLs}\left(\varepsilon_{CU,CONFINED}, \varepsilon_{SU}\right) \end{pmatrix}$, V_{NC}
GLOBAL PARAMETERS		
DL	**SD**	**NC**
$\frac{d}{H} = 1\%$	$\frac{d}{H} = 2\%$	$\frac{d}{H} = 4\%$

Although Eurocode 8 – Part 3 (EN 8 – 3, 2005) states that existing RC structures should be checked in terms of deformation capacity through the chord rotation, and the cyclic shear resistance, many other parameters concerning with all the limit states were defined. The Limit State Limited Damage (DL) includes: ε_c, the strain at the peak of the maximum compressive strength of the concrete cover, set up at 0.2% and after which there is significant decay of the compressive strength of the concrete cover ; ε_{SY} the steel yielding which corresponds to the ratio between the yielding stress and the elasticity modulus of the rebar; $M_{y,BMs}$ the moment yielding of flexural-dominated RC elements which is commonly computed by using the elastic segment of the M-φ curve according to the Eurocode 8, and it is the minimum between the bending moment considering the yielding of the tension rebars and the apparent "elastic strain limit of the concrete"; $\left(N_{y,cols}, M_{y,cols}\right)$, seismic events exert horizontal forces on RC structures which increase the stress levels in the RC components in terms of axial force and bending moment; thus, the interaction surface of the M, N pair corresponding at the ε_C and ε_{SY} was built to check the stress levels of all columns at the limited damage. The Limit State of Significant Damage (SD) includes: $\varepsilon_{CU,COVER}$, Mander et al. (1988) and Chang et al. (1992) said that the ultimate strain of the unconfined concrete should zero the compressive strength of the cover concrete, which indicates the cover spalling, but they suggested values from the literature while, here, the formulation provided by Biskinis et al. (2007) and reported by Fardis (2009) for unconfined concrete under cycling loading is used:

$$\varepsilon_{CU,COVER} = 0.0035 + \left(\frac{10}{d}\right)^2 \tag{18}$$

Biskinis and Fardis (2009) conducted an experimental campaign for evaluating the ultimate curvature of RC members. They observed that the ultimate curvature for RC elements was reached by the rupture of the tension reinforcement and, this leads to a conclusion that the elongation of steel rebars under cycling loads is on average $\frac{3}{8}\varepsilon_{SU}$; $M_{U,BMs}\left(\varepsilon_{CU,COVER}, \frac{3}{8}\varepsilon_{SU}\right)$, represents the ultimate moment computed for flexural-dominated RC components according to the Eurocode 8 considering as ultimate strains $\varepsilon_{CU,COVER}$ and $\frac{3}{8}\varepsilon_{SU}$; $\left(N_{U,COLs}, M_{U,COLs}\right)$ is the interaction surface of the M, N pair calculated considering as ultimate strains $\varepsilon_{CU,COVER}$ and $\frac{3}{8}\varepsilon_{SU}$ respectively. Finally, the limit state of Near Collapse (NC) includes: $\varepsilon_{CU,CONFINED}$, the confinement is typically neglected in seismic design. However, confined concrete is a key point when an earthquake occurs as it allows concrete members to undergo larger inelastic deformation compared to the design value of 0.35%. Here, the minimum between the ultimate strain defined by Razvi et al. (1992) and formulation provided by Biskinis et al. (2007) and reported by Fardis (2009) for confined concrete under cycling loading was used:

$$\varepsilon_{CU,COVER} = 0.0035 + \left(\frac{10}{d}\right)^2 + 0.4\,\frac{p}{f_{cc}}; \tag{19}$$

where p is the confinement coefficient and f_{cc} is the compressive strength of the concrete core; ε_{SU} is the ultimate strain corresponding to the steel reinforcement softening which is typically set up at 1%; $M_{U,BMs}$ is the ultimate Moment for flexural-dominated RC members according to the Eurocode computed with the strain values at $\varepsilon_{CU,CONFINED}$ and ε_{SU}; $\left(N_{U,COLs}, M_{U,COLs}\right)$ is the interaction surface of the M, N pair corresponding at the $\varepsilon_{CU,CONFINED}$ and ε_{SU}. Local parameters are reduced to account for the level of corrosion exploiting the relationships provided for concrete and steel reinforcements. During the analysis, the first element that reached the limit condition is given and, then, the minimum value among the local parameters defined in Table 4 checked against the global parameter for each Limit State.

Furthermore, another parameter was evaluated in the Pushover Analyses, the ductility which quantifies two important response characteristics: the capacity of the structure to undergo inelastic deformation with acceptable stiffness and strength; the plastic redistribution of actions and the dissipation of the earthquake energy. Additionally, this study includes the overstrength, which quantify the actual strength in excess against a seismic event, and the translation ductility to assess damage tolerance and therefore resiliency into the structure. Overstrength and ductility are defined as follows:

$$\mu_\delta = \frac{\delta_u}{\delta_y} \tag{20}$$

$$\Omega_\delta = \frac{F_u}{F_y} \tag{21}$$

where F_y represents once the yield point of an equivalent elasto-plastic system with reduced stiffness computed as secant stiffness equal to 75% of the maximum lateral force to evaluate the global behaviour of the RC structure and, then, the F_y corresponding to the value of the first chord rotation reached in the building to evaluate a local response; F_u can be computed as either the shear corresponding to the first fracture or buckling and the shear corresponding to the minimum of the local parameters defined in the limit State Near Collapse; δ_y is the displacement corresponding to the yield force F_y; δ_u is the displacement corresponding to F_u.

7.2 ELASTIC DYNAMIC RESPONSE (MODAL ANALYSIS)

The modal analysis is extremely important in the study of the dynamic properties and identification of the vibration modes of a structural system. Modes are defined by the modal parameters such as frequencies and mode shapes. Here, the modal analyses were used to evaluate the elastic response when the existing RC structure is exposed to different levels of corrosion. Figure 13 depicts the first three main periods of the structure without corrosion, while Figures 14 show the comparison between different exposures and levels of corrosion with the uncorroded case:

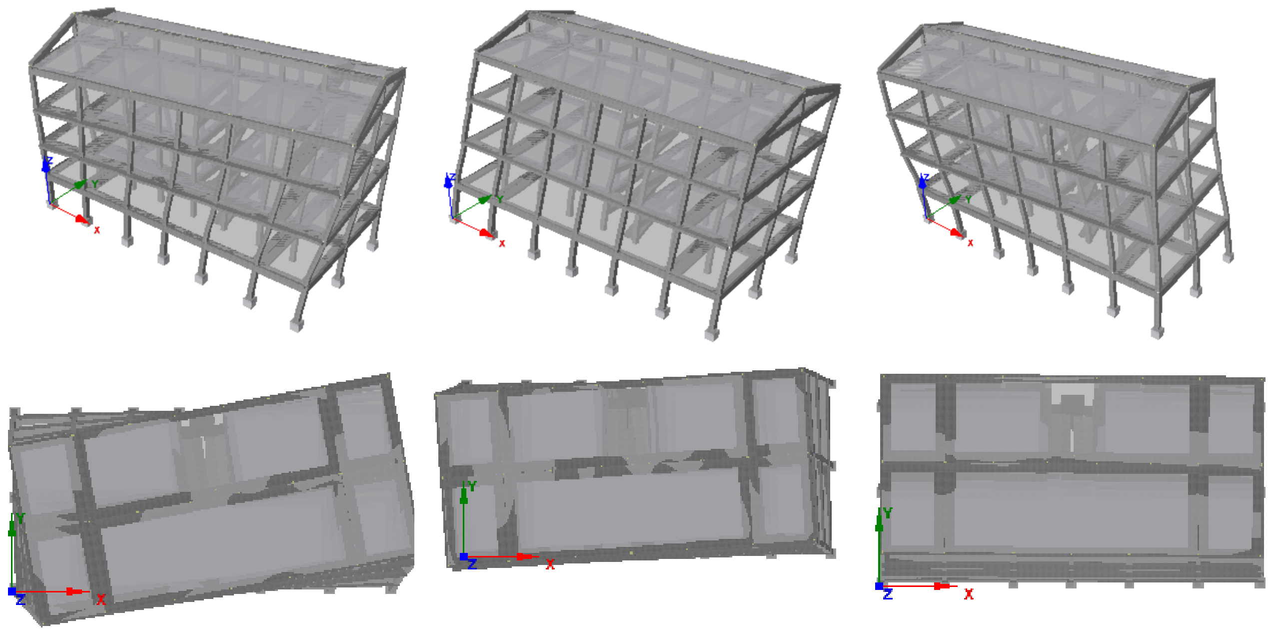

T_1 = 0.784 sec T_2 = 0.720 sec T_3 = 0.683 sec

			MASS PARTICIPATION FACTOR					
CR[%]		**Periods[secs]**	**[Ux]**	**[Uy]**	**[Uz]**	**[Rx]**	**[Ry]**	**[Rz]**
0	**T_1[secs]**	0.784	9.4%	0.0%	0.0%	0.0%	1.0%	69.1%
	T_2[secs]	0.720	69.0%	0.2%	0.0%	0.0%	4.9%	9.8%
	T_3[secs]	0.683	0.1%	75.8%	0.0%	14.3%	0.0%	0.1%

Figure 13. The main mode of vibrations of the RC structure

Results clearly showed an increase in the natural frequency of the RC structure when exposed to corrosion. Figures 14 notably illustrate that the RC building with full-sided corroded had an increase in the fundamental frequency of 6.7% and 7.3% with a corrosion rate of 15% and 20% respectively. Conversely, the increase in the fundamental frequency of the RC building with full-sided corroded beams was 3.7% and 4.1% with a corrosion rate of 15% and 20%. Furthermore, It can be observed a relevant increase in the natural frequencies when the entire building was exposed to corrosion. The main reasons for the decay of the natural frequencies can be found in the mass loss of RC components and stiffness degradation due to cracking, which lead to an increase of the mass participation factor along the main direction of the mode shape without changing the elastic response of the building. However, these three scenarios do not represent the real case of an RC building exposed to corrosion as the inside is protected by infills and the corrosion path could stop on the external side. It should be stressed that the testbed building was modelled without considering infills, which will possibly affect the fundamental period and mode shapes of the RC framed structure, and therefore increasing the dramatic effect of corrosion (Fardis and Calvi, 1994; Kappos and Ellul, 2000; Kose, 2009, among the others). Only the external RC components, both beams and columns, can be reasonably exposed to aggressive agents which penetrate through RC elements and lower the mechanical properties of both the concrete and steel reinforcements. As a result, the penetration attack was considered on three-sides of the corner columns and two-sides for the other RC components respectively.

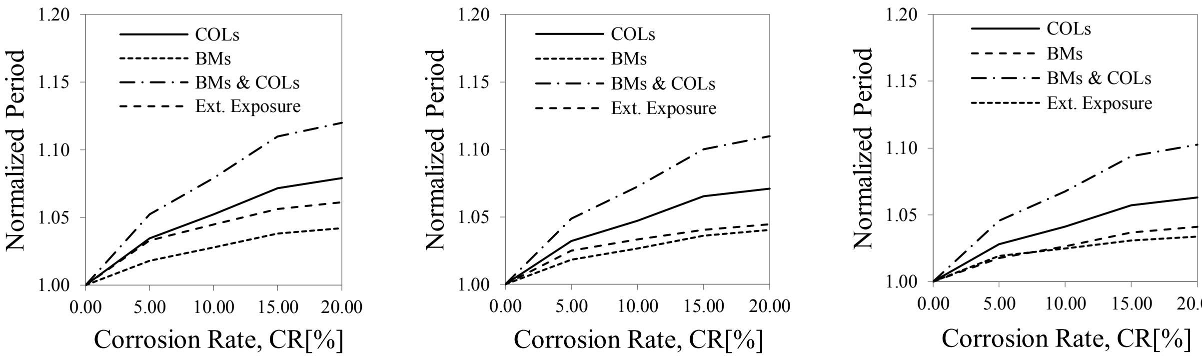

Figure 14. Normalized Period vs Corrosion Rate. a) T_1=0.784 secs; b) T_2=0.720 secs; c) T_3=0.683 secs

Figures 14 show interesting results for external exposure as there is a reduction of the natural frequency and a change in the mass participation factor. As a result, the mode shape tends to change and even if the first mode remains torsional, there is a relevant decrease in the mass participation factor along the main direction of the mode shape which could mean that the RC structure is shifting its natural mode. Finally, damage due to the corrosion penetration strongly alters the dynamic properties of an RC structure which lead to a change in the Eigen-parameters such as the natural frequency and, in some cases, the modal shapes, and even if no experimental campaign can be found in the literature to compare the results, these numerical analyses can be very useful in inspiring future research on the elastic response of RC structures and components exposed to different levels of corrosion.

7.3 INELASTIC STATIC RESPONSE: PUSHOVER ANALYSIS

The non-linear Static Analysis, also known as Pushover Analysis (PA), is widely used in seismic resistance assessment as a reliable alternative to the non-linear dynamic analysis for the evaluation of the inelastic response of an RC structure under a lateral loading pattern. The main outcome of the PA is the capacity curve which is a graphical representation of the Base Shear against the target displacement located at the top floor of the structure. The inelastic behaviour of RC components has been herein simulated by Fiber-based frames. The PAs were performed in both directions, x and y, considering five levels of corrosion rate (CR [%] = [0, 5, 10, 15, and 20]) and different horizontal loading patterns according to the Eurocode 8 – Part 3(EN 8-3, 2005): a) the mass distribution according to the modal shapes of the RC structure (Adaptive Pushover Analysis); b) uniform pattern based on lateral forces proportional to the mass of each floor; c) lateral loads based on the acceleration distribution proportional to the mode shape (x and y). The evaluation of the performance of the existing RC structure was conducted using a technical code., i.e. Eurocode 8 – Part 3(EN 8-3, 2005). Particularly, the seismic demand was here expressed through the use of the Drift Limits stated in Eurocode (EN 1998-1 (2004) with additional provisions (FEMA 356, 2000) for the Limit States of Limited Damage (LD), Significant Damage (SD) and Near Collapse (NC).

7.3.1 PUSHOVER ANALYSIS OF THE RC STRUCTURES WITH COLUMNS EXPOSED TO CORROSION

Non-linear Static analyses were performed to evaluate the seismic performance of the existing RC building when columns are exposed to different levels of corrosion. The mechanical properties of both the steel reinforcements (ST) and the concrete (CO) were reduced using the relationships (4), (8) and (9). Figures 15a, 15b and 15c illustrate the base shear strength against the roof drift ratio for all horizontal loading patterns. Results from the non-linear static analyses show that the seismic performance of the building is directly related to the lateral load pattern utilized. In fact, different responses for the capacity curves were obtained using the three loading patterns previously defined. Figures 15 clearly showed a significant reduction in both the base shear and the ductility with the increase of the corrosion rate. In particular, high levels of corrosion, between 15% and 20%, reduced the base shear by 39% and 44% along the x-axis, while the structure was not able to withstand horizontal loads greater than 10% of the seismic weight along the y-axis. Moreover, Figures 15 demonstrated that the structure could not comply with the seismic capacity, according to the limit states (Global Parameters) defined in Table 4,owing to a highly corrosive environment. Thus, the structure could not resist extensive damage and fulfil the performance level required by the Limit State of Near Collapse (NC) with corroded elements and the Limit State of Significant Damage (SD) with a corrosion rate of 20%. To satisfy the limit states, the minimum among the local parameters (Table 4), which has been reduced according to the level of corrosion, must be greater than the global parameters (Table 4), which would allow the RC structure to perform its intended function throughout its lifetime. Cover spalling of the column seems to govern the limit state LD with the increase of corrosion rate, while concrete cover failure and concrete core failure are the first consequences for SD and NC for highly-corrosive environments. Since corrosion was applied only on the columns, repair-solutions should primarily focus on these structural elements.

All lateral loading patterns showed a significant reduction of the ductility with the increase of corrosion. As a result, large levels of corrosion forced the building to shift its failure mode from ductile to brittle, which can be seen in Figure 15a, 15b and 15c when the corrosion rate is between 15% and 20% in both directions (x and y). Table 5 summarizes the results obtained for the ductility, overstrength and behaviour factor with the increase of the corrosion rate. It is evident that there is a relevant decrease in the ductility by more than 40% when the corrosion rate was between 15% and 20%, which may justify the change in the failure mode of the RC structure.

Furthermore, it can be observed a significant decrease in the overstrength with the maximum increase of the corrosion rate by 40% and 64%, along x and y, respectively.

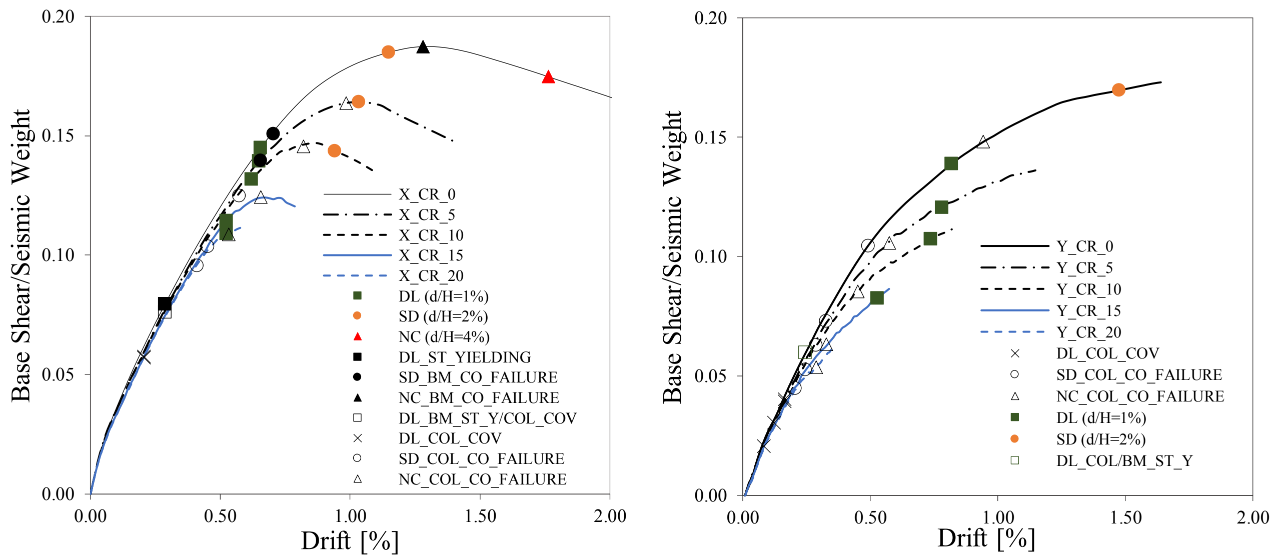

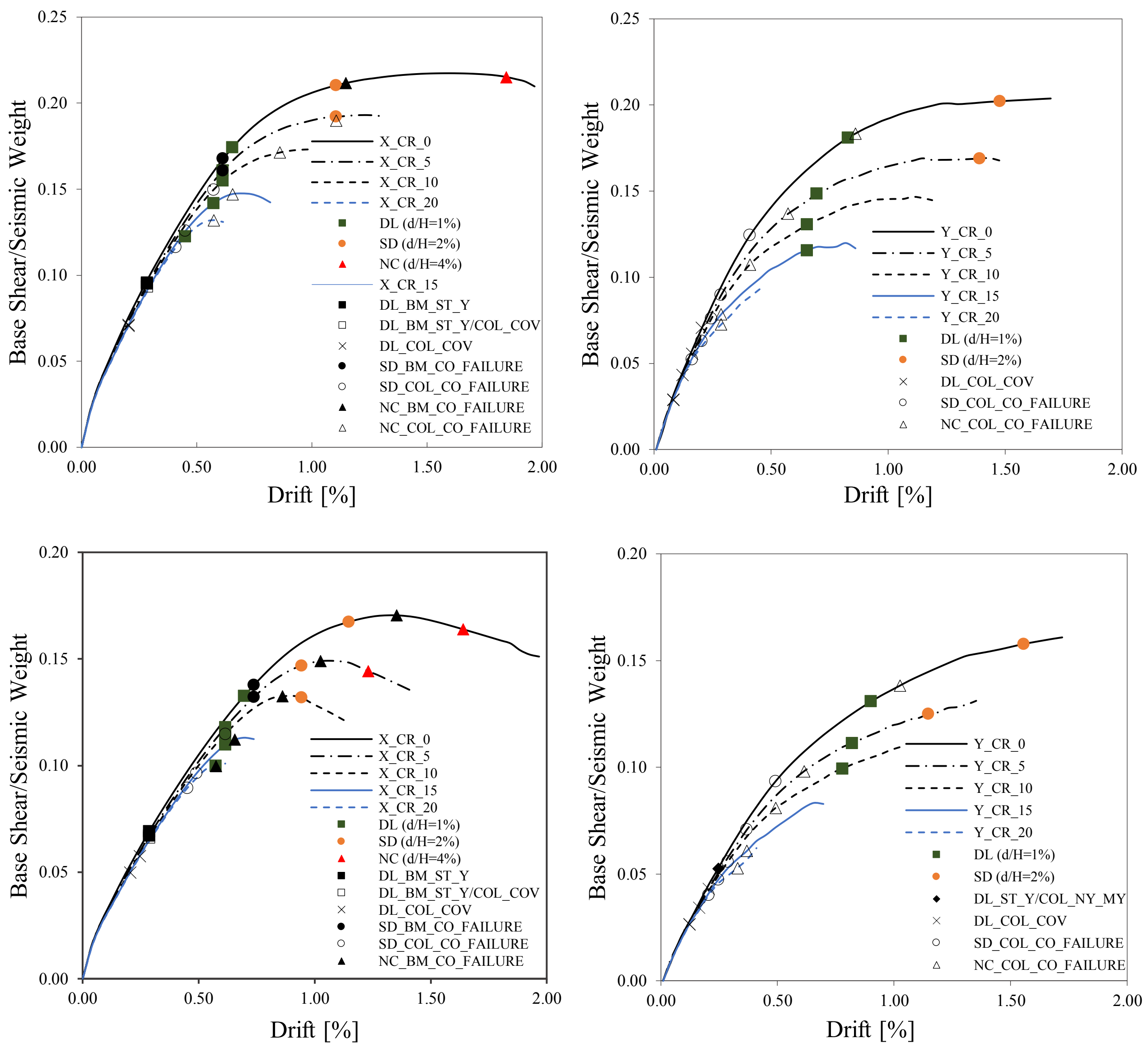

Figure 15. a) Adaptive Pushover (X-Y Directions); b) Lateral Loading proportional to the acceleration distribution (X-Y Directions); c) Uniform Pattern (X-Y Directions)

Table 5. Translation Ductility, Overstrength and Behaviour Factors.

CR [%]	μ_x	μ_y	Ω_x	Ω_y	$q_{x\text{-Mean}}$	$q_{y\text{-Mean}}$
0	2.43	1.87	1.73	1.59	4.20	2.77
5	2.01	1.78	1.52	1.25	3.79	2.15
10	1.82	1.64	1.36	1.01	3.01	1.92
15	1.55	1.40	1.15	0.78	1.82	1.22
20	1.36	1.02	1.03	0.57	1.43	0.57

Similarly, Table 5 describes the values of the q-factors with the increase of the corrosion rate. Results show that there is a significant reduction (66%) along the x-axis and a dramatic decay (79%) along the y-axis as the corrosion rate goes up to 20%.

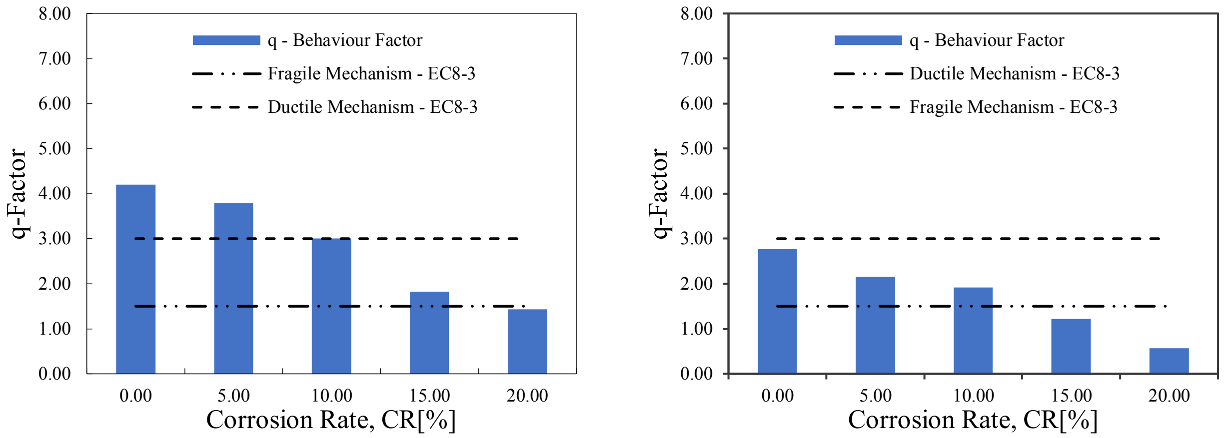

Figure 16. q-Factor vs Corrosion rate (Y-Axis & X-axis)

Moreover, highly corroded RC building (10%) forced the structure to change its failure mode, and, therefore, to not comply with the ductile failure mechanisms specified by the Eurocode 8 – Part 3(EN 8-3, 2005). The q-factor values are given in terms of mean between all lateral loading patterns used for the PAs.

7.3.2 PUSHOVER ANALYSIS OF THE RC STRUCTURES WITH BEAMS EXPOSED TO CORROSION

In this section, the seismic performance of the testbed building with corroded beams was investigated. Noticeably, results showed a slight reduction of the base shear and the ductility in both directions. The base shear decreased by 19% with a corrosion rate of 20% for all the lateral loading patterns, while the structure was able to withstand horizontal load with a decrease of base shear lesser than 15% along the y-axis. Furthermore, Figures 17 show that the structure was able to comply with the seismic performance required by the Limit States for all the lateral loading patterns until a corrosion rate of 15%, while was not able to fulfil the seismic requirements along the y-axis regardless the corrosion rate. In terms of ductility, there is a slight reduction even when the structure was exposed to highly corrosive environments allowing the building to sustain seismic loads, resist extensive damage and contain the earthquake energy. Steel yielding in beams is the first consequence of the corroded beams, which becomes critical for corrosion levels greater than 10% whereas the structure cannot satisfy the Limit State DL. Although the columns were not exposed to corrosion, cover concrete failure in columns is the first limit condition for the Limit State SD, while cover concrete failure in beams seems to govern this Limit State only for high levels of corrosion. The failure of the concrete core in beams and columns was the local parameter, among the others, checked against the performance levels required by the Limit State NC. It is also noteworthy that the seismic performance, as well as the Limit State checks, are directly related to the different lateral loading patterns. The main observations that arise from the response of each pushover curve are that local parameters developed in different points for different lateral loads, and, in some cases, they do not comply with the specific requirements specified by modern seismic-based technical codes. Although beams mainly seem to undergo damage, repair-solutions should also focus on columns that reached the limit conditions, especially for the limit states NC and SD.

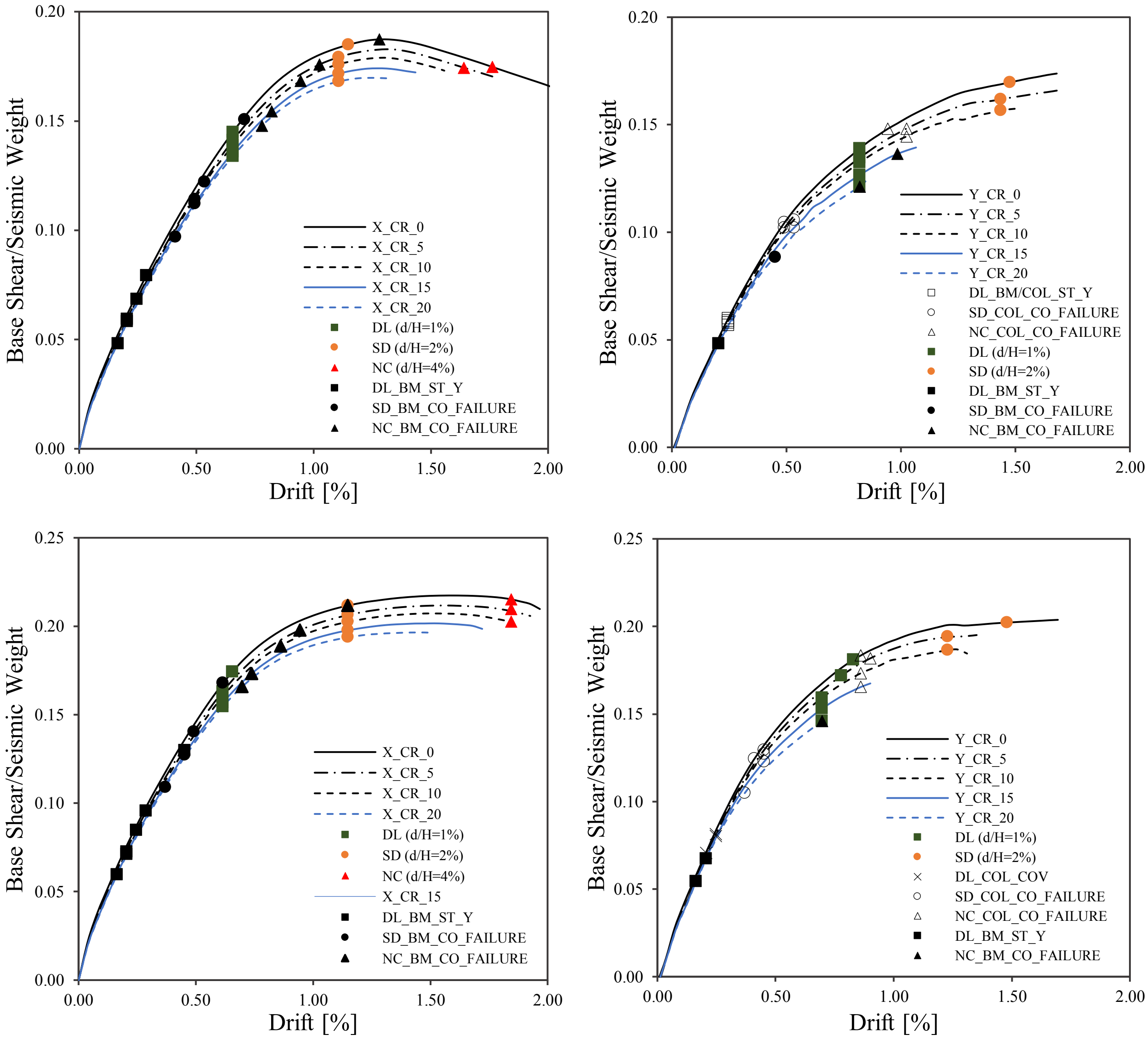

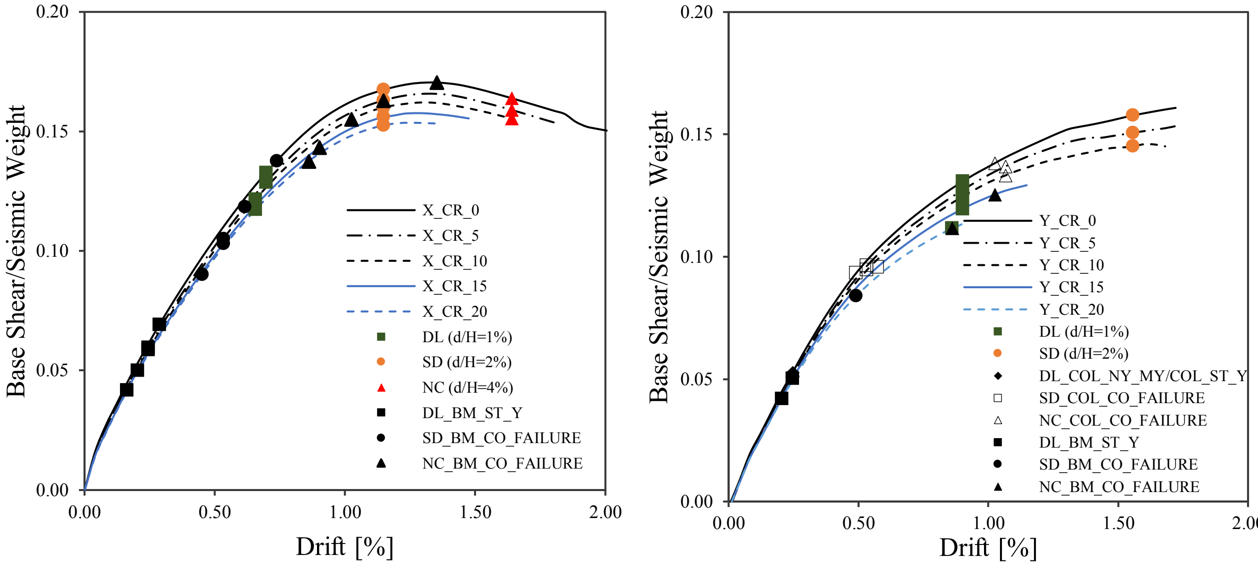

Figure 17. a) Adaptive Pushover (X-Y Directions); b) Lateral Loading proportional to the acceleration distribution (X-Y Directions); c) Uniform Pattern (X-Y Directions)

Table 6 sums up the results for the overstrength, ductility and behaviour factor with the increased level of the corrosion rate. It can be noted a slight decrease in the ductility along the x-axis while a relevant decrease of 44% along the y-axis. The reduction of the overstrength appears to be negligible in both assumed directions (x and y). The cause of this minor decrease can be found in the local parameters where the corrosion attack does not reduce substantially the properties of the beams, and the first limit condition was reached in the columns which are uncorroded. The reduction of the yielding stress in beams caused by corrosion can enhance the dissipation of the RC framed structures. When beams yield earlier than columns, then the energy dissipation capacity of the framed structure is higher. This case study demonstrated that the damage caused by corrosion in beams is lower In comparison with the scenario where only columns were subjected to corrosion, and the building is still able to exploit its shear capacity. As a result, if corrosion occurs, the RC columns are the first elements to be retrofitted as the shear capacity dramatically decreases by half of its initial capacity compared to the small shear reduction of the RC building with corroded beams.

Table 6. Translation Ductility, Overstrength and Force-Reduction Factors.

CR [%]	μ_x	μ_y	Ω_x	Ω_y	$q_{x\text{-Mean}}$	$q_{y\text{-Mean}}$
0	2.43	1.87	1.73	1.59	4.20	2.77
5	2.15	1.77	1.69	1.53	3.63	2.72
10	2.11	1.61	1.65	1.45	3.20	2.42
15	1.91	1.44	1.61	1.29	2.89	1.78
20	1.80	1.05	1.57	1.16	2.63	1.41

Furthermore, Table 6 shows the variation of the q-factor with the increase of the corrosion percentage. There is a consistent reduction of the q-factor, 37% and 49% in both directions, as the corrosion penetration goes deeper into the RC members.

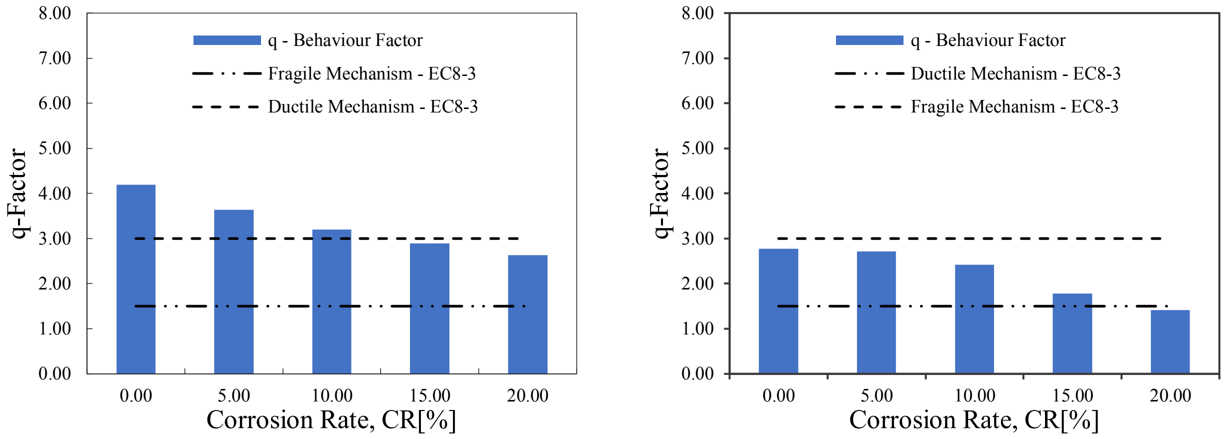

Figure 18. q-Factor vs Corrosion rate (Y-Axis & X-axis)

The trends in Figures 18 show that corroded beams have a less impact in comparison with corroded columns. Particularly, the building is still able to exhibit a ductile failure mechanism along the x-axis, while cannot comply with the limit specified by the Eurocode along y-axis. The last observation indicates that the impact of corrosion is strongly affecting the deformation capacity of the building.

7.3.3 PUSHOVER ANALYSIS OF THE RC STRUCTURE WITH BEAMS AND COLUMNS EXPOSED TO CORROSION

The seismic performance of the entire structure exposed to corrosion is discussed hereafter. Beams and columns were subjected to a full-sided exposure which entails the maximum reduction of the compressive strength of an RC component. Results in Figures 19 clearly showed a significant reduction in both base shears and ductility for all the lateral loading patterns. Low and high levels of corrosion considerably reduced the capacity of the structure to resist seismic loads and dissipate the earthquake energy with extensive damage and unacceptable strength. The corrosion rate of 5% reduced the base shear by 20%, while highly corrosive environments, between 15% and 20%, weakened the structure in both directions changing its failure mode from ductile to brittle. In addition to this, the building was not able to fulfil the seismic requirements for the Limit State NC, and for the limit states SD and DL with a corrosion rate of 20%. The ductility was strongly affected by the increased level of corrosion, especially along the y-axis. As a result, a change in the failure mode of the structure was noted. The building with a corrosion level greater than 10% could not withstand large inelastic deformation showing a brittle behaviour and large damage. In terms of local parameters, steel yielding of beams along the x-axis and cover spalling of columns along the y-axis are the main causes of the increasing corrosion level for all the lateral loading patterns and, particularly, steel yielding of the beams does not comply with the limit state DL when corrosion level is greater than 10% along the x-axis. At the same time, the cover spalling of the columns does not respect the seismic requirement for DL regardless of the corrosion percentage. Concrete failure of the cover for columns and beams remains the main parameter, along the x-axis, to be checked against the Limit State SD with the increase of the corrosion penetration while columns become more vulnerable along the y-axis whereby the building is noticeably not able to fulfil the seismic requirement for SD when corrosion occurs. The Limit state NC was governed by the concrete core failure of the columns in both directions. As a result, a repair solution should focus on strengthening the columns, which are the main RC components to be vulnerable when the entire building is exposed to highly aggressive environments. The reduction of the base shear is obviously greater than the other case-studies presented so far as the corrosion attack is acting on the entire structure internally and externally and, particularly, equals to more than 55% compared to 39% and 20% for only corroded columns and only corroded beams respectively.

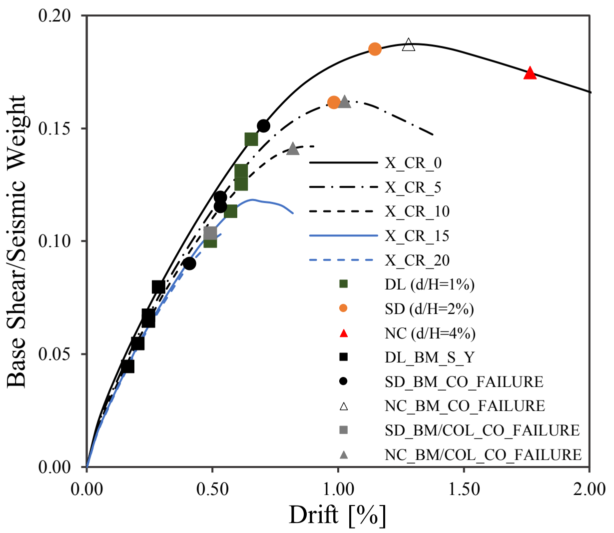

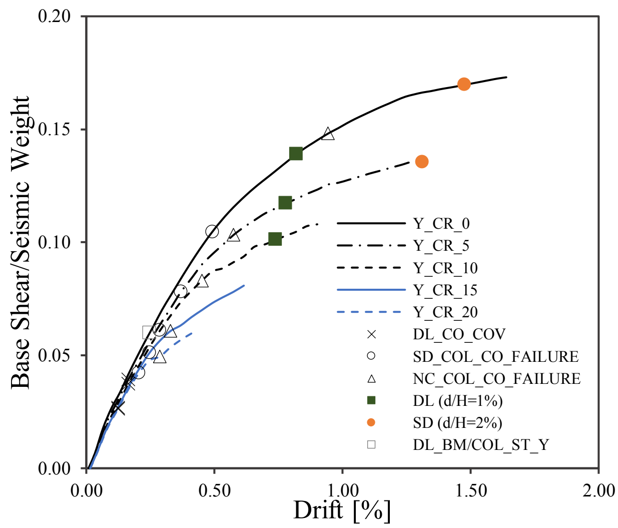

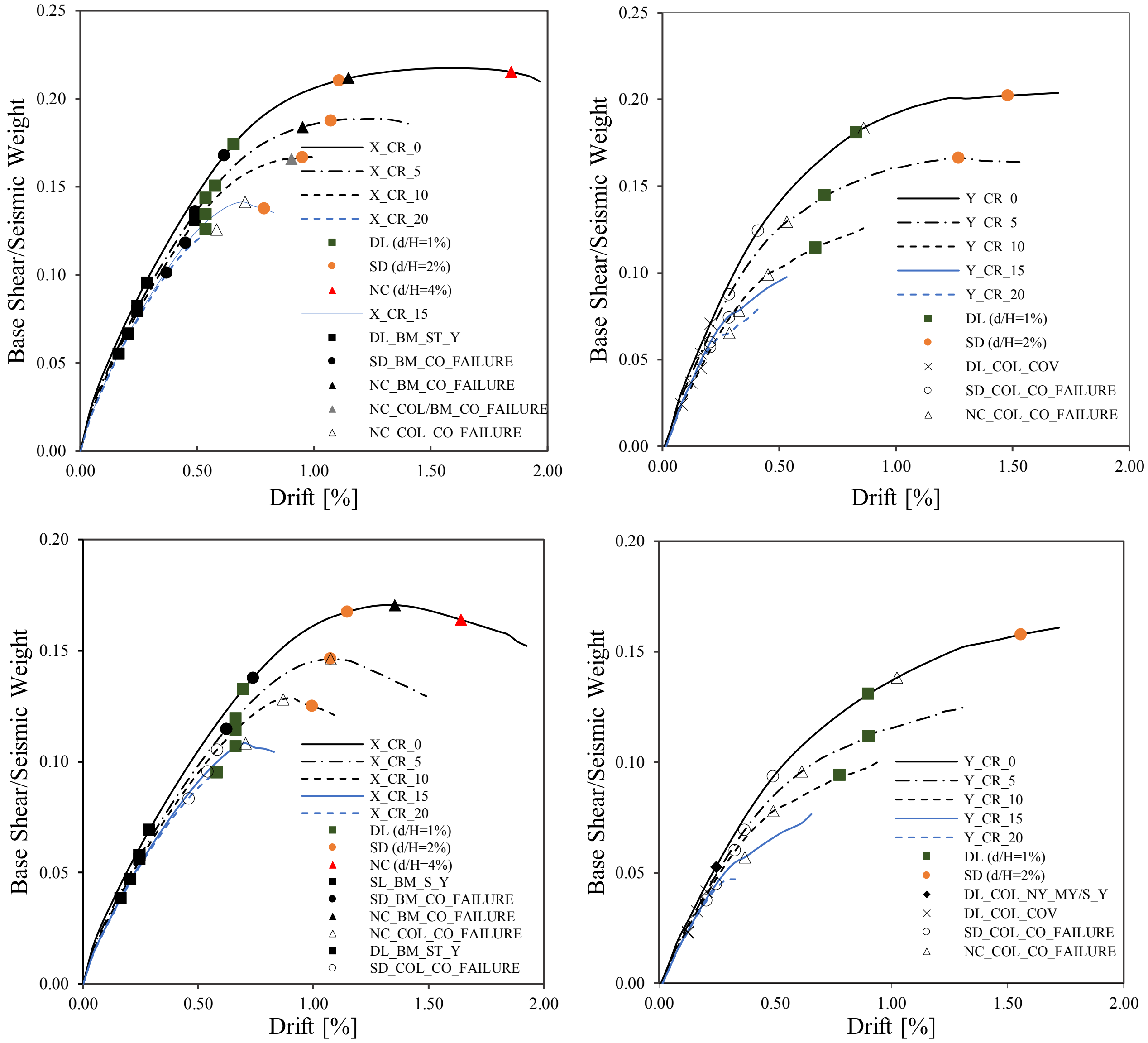

Figure 19. a) Adaptive Pushover (X-Y directions); b) Lateral Loading proportional to the acceleration distribution (X-Y directions); c) Uniform Pattern (X-Y directions)

The global translation ductility significantly decreased in both directions, x and y, as can be seen in Table 7. Particularly, the increased level of corrosion reduced the capacity of the structure to exploit its resistance to inelastic deformation between 48% and 32%, respectively. In addition, Table 7 illustrates the reduction of the global overstrength with the increase of the corrosion rate.

Table 7. Translation Ductility, Overstrength and Force-Reduction Factors.

CR [%]	μ_x	μ_y	Ω_x	Ω_y	$q_{x\text{-Mean}}$	$q_{y\text{-Mean}}$
0	2.43	1.87	1.73	1.59	4.20	2.77
5	2.01	1.64	1.49	1.25	2.96	2.12
10	1.59	1.58	1.31	1.00	2.04	1.58
15	1.63	1.40	1.09	0.75	1.79	1.05
20	1.26	1.27	0.95	0.55	1.19	0.70

From the results in Table 7, the behaviour factor significantly decreased with the increased level of corrosion, which does not allow the structure to exploit its initial inelastic deformation capacity. For a level of corrosion lesser than 10%, the reduction was 40% along the x-axis and 42% along the y-axis, while for high levels of corrosion the q-factor decreased by half of its initial uncorroded value. This scenario is undoubtedly the worst case compared to the above-illustrated two case-studies because the corrosion is applied both on columns and beams. However, the columns are still the primary members to be retrofitted as the performance points are reached in these components earlier than beams. The reduction of the overstrength of the RC building cannot prevent the RC building from moving to brittle failure modes without any warning.

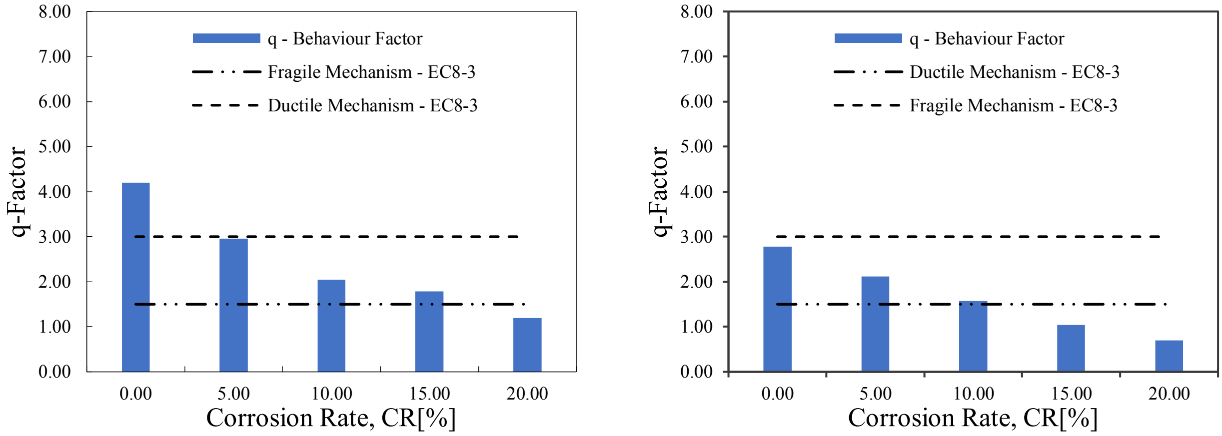

Figure 20. q-Factor vs Corrosion rate (Y-Axis & X-axis)

Figure 20 illustrates the values of the behaviour factor against the corrosion rate compared with the failure mechanisms specified by the Eurocode 8. It is evident that the entire structure exposed to corrosion shifts its failure mode from ductile to brittle, even for low-corrosive environments (CR [%] =5%)

7.3.4 PUSHOVER ANALYSIS OF THE RC STRUCTURE WITH EXTERNAL EXPOSURE

Albeit, all the scenarios presented so far are technically interesting because it allows to evaluate the seismic performance of an existing RC building with some components exposed to corrosion, they do not correspond to a real case as internal infills protects ordinary buildings. As a result, only the external components are directly exposed to destructive physical and chemical agents.. In this section, external columns and beams were subjected to the corrosion attack and, particularly, the mechanical properties of the corner columns were reduced considering a three-sided attack, while a two-sided attack was considered for the beams and the remain columns. These two case-attacks are globally and locally different from the other scenarios above-mentioned as the building could still exploit the strength of uncorroded RC components, and the reduction of concrete's compressive strength is less because of three and two-sided corrosion penetration if compared to a full-sided attack. Furthermore, the model does not account for any additional effects from infilled walls. Results in Figures 21 showed a moderate decrease of the base shear in both directions, which seem to linearly reduce until the corrosion rate of 20% with a maximum reduced base shear equal to the 14% of the seismic weight with a base shear loss around 27% compared to the uncorroded building. The ductility is obviously affected by the highly corrosive environments without substantially changing its failure mode. Furthermore, the structure is able to comply with the seismic performance required by the limit states along the x-axis with the corrosion rates lower than 10%, while corrosion rate greater than 10% do not allow the structure to reach the limit State NC along the y-axis. In terms of local parameters, cover spalling and Ny-My pair for columns are the main consequences of the increase in the corrosion rate, while steel yielding for beam becomes critical with a highly corrosive environment. The structure does not fulfil the limit state DL for a corrosion rate greater than 10% for all the lateral loading patterns and in both directions.

On the other hand, concrete cover failure and concrete core failure govern the limit states SD and NC, which is critical with a corrosion rate between 15% and 20% along the x-axis and greater than 5% along the y-axis. Table 8 shows that the global translation ductility decreased by 20% along the y-axis, which still allows the structure to resist large inelastic deformation, and significantly by 34% along the y-axis with the increase of the corrosion rate. The global overstrength demonstrated a slight decay with the increased level of corrosion. The reduction of the shear strength appears to be lesser compared to the building with corroded columns, and greater with corroded beams. Finally, even if the impact of corrosion on the ductility is still significant, the existing building is more able to dissipate energy and exploit its inelastic deformation capacity compared to the other three exposure-cases.

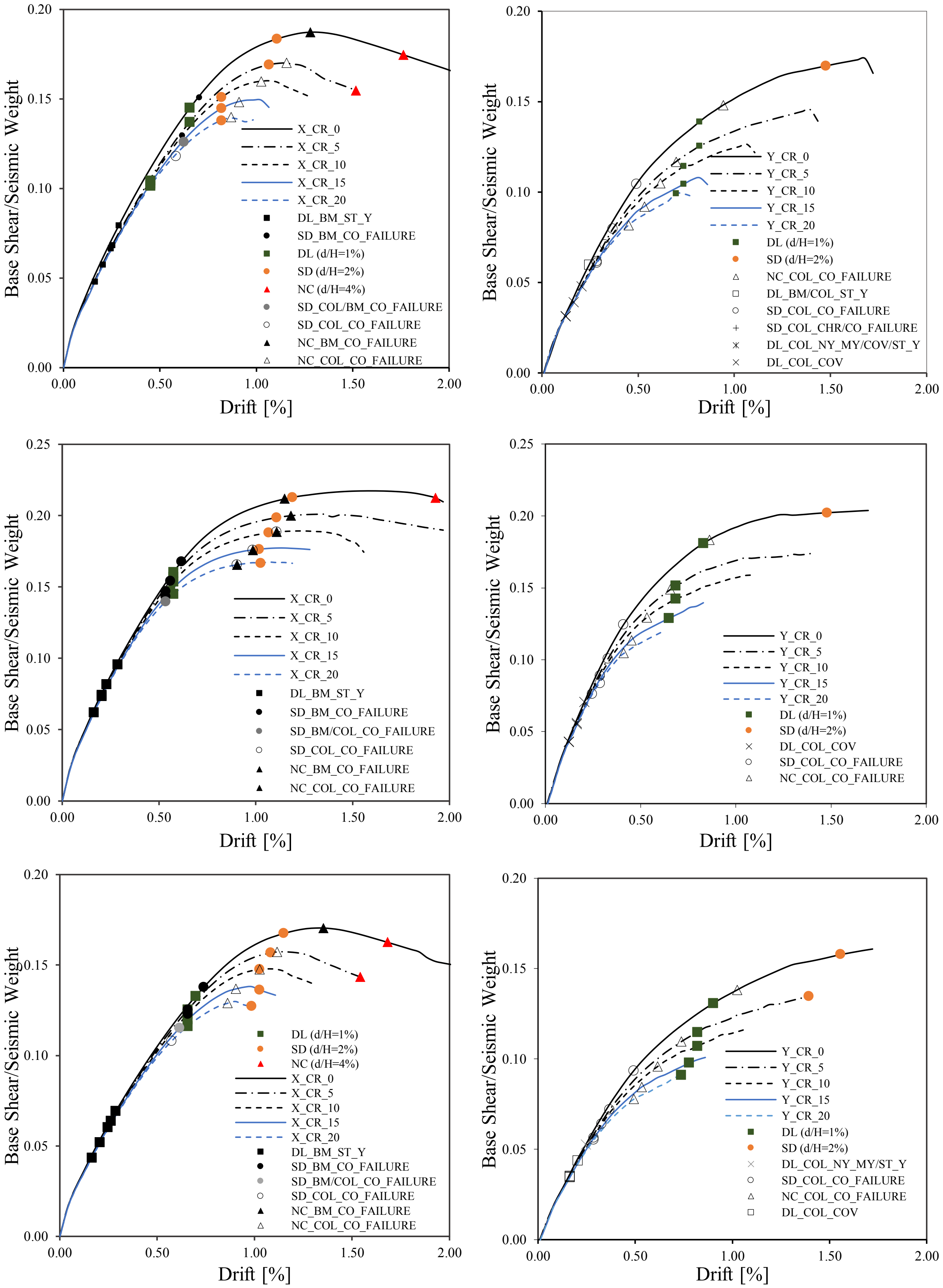

Figure 21. a) Adaptive Pushover (X-Y directions); b) Lateral Loading proportional to the acceleration distribution (X-Y directions); c) Uniform Pattern (X-Y directions)

Table 8 summarizes the values of the overstrength, the translation ductility and the behaviour factors obtained from the nonlinear static analyses. The latter parameters are given as an average of all lateral loading patterns herein considered.

Table 8. Translation Ductility, Overstrength and Force-Reduction Factors

CR [%]	μ_x	μ_y	Ω_x	Ω_y	$q_{x\text{-}Mean}$	$q_{y\text{-}Mean}$
0	2.43	1.87	1.73	1.59	4.20	2.77
5	2.04	1.73	1.57	1.34	3.16	2.32
10	1.82	1.62	1.48	1.17	2.66	1.89
15	1.65	1.53	1.38	1.00	2.25	1.47
20	1.60	1.62	1.29	0.92	2.06	1.54

The global ductility of existing RC buildings was checked with the values defined by EC8-3, 1.5 and 3.0 for fragile and ductile mechanisms, respectively.

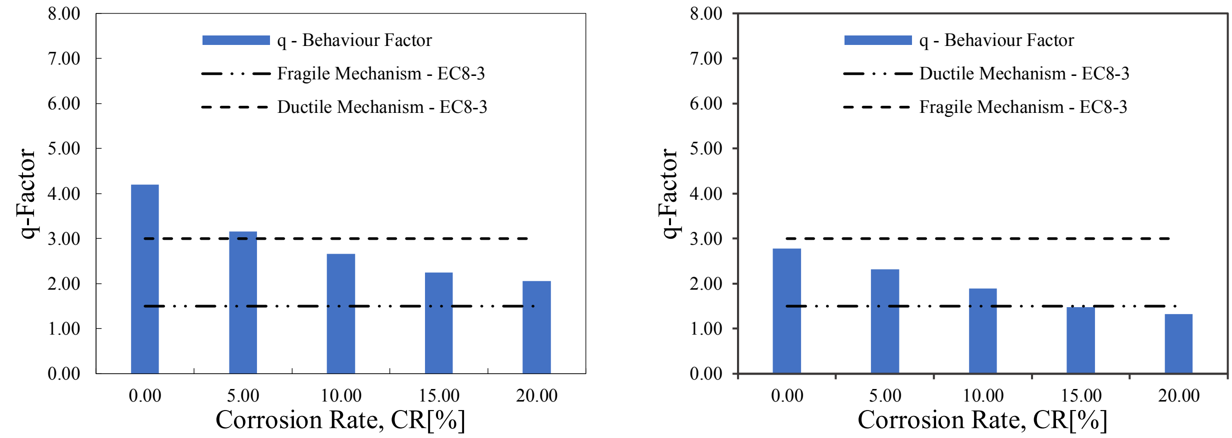

Figure 22. q-Factor vs Corrosion rate (Y-Axis & X-axis)

Figures 22 show the q-factor for different levels of corrosion. Results obviously demonstrated that the impact of corrosion lowers the q-factor in both directions forcing the analyzed existing building to brittle failures, especially for levels of corrosion greater than 10%. The maximum reduction of the q-factor was 34% for a corrosion rate of 20%. Compared to the results obtained from the previously investigated cases, the behaviour factors are greater in both directions, which means that the real case does not represent the worst scenario, and the uncorroded RC members may help to preserve the safety.

7.4 NONLINEAR DYNAMIC ANALYSIS

7.4.1 EARTHQUAKE INPUT CHARACTERISTICS

Nonlinear Dynamic analysis is commonly used to predict the inelastic response of structures subjected to earthquake ground motions. The results are herein presented in terms of Mean-Relative

Storey-Displacements, Maximum Base Shear and Maximum Displacement at the top of the building (Figure 8a and Figure 8b) and checked against the Drift Limits stated in Eurocode (EN 1998-1 (2004) and provisions (FEMA 356, 2000). All the storey-displacements have been combined using the following formulation:

$$D_{tot} = \sqrt{D_x^2 + D_y^2} \tag{19}$$

The time-history analyses were carried through the selection of real-ground motions (Eurocode 8-Part 1 Sec. 3.2.3) using the spectrum-compatibility rules. A reliable software called REXEL [Iervolino et al. (2010)] has been utilized for generating the spectrum-compatibility signals. The selection of seven real-ground motions was conducted using the structural periods T_2 and T_3 for the x-axis and y-axis, respectively, and for all the limit states. Finally, the ground motions were then chosen based on the greatest average PGAs among the two structural periods and inserted into the model. Table 9 shows the seismological parameters of the natural ground motions for each limit state, such as PGA, duration, predominant period and arias intensity.

Table 9. Seismological Parameters of the Ground Motions

Limit State	Waveform ID	Mw	PGA_X [m/s^2]	PGA_Y [m/s^2]	$Duration_X$ [sec]	$Duration_Y$ [sec]	AI_X[m/sec]	AI_Y[m/sec]	Pred. Per. X [sec]	Pred. Per. Y [sec]
Limited Damage	439	6.70	1.79	1.80	8.83	10.47	30.21	25.14	0.30	0.36
	581	5.40	1.72	1.96	8.92	9.02	18.81	19.34	0.46	0.40
	592	6.00	1.95	2.18	9.71	11.56	47.18	41.83	0.16	0.08
	4343	7.60	1.08	1.12	39.45	38.99	23.98	31.92	0.64	0.44
	602	6.00	1.14	1.07	11.73	11.45	8.23	9.58	0.14	0.14
	1726	6.30	2.16	2.64	13.01	13.24	86.24	96.86	0.66	0.52
	1257	7.60	2.90	2.39	32.15	33.46	146.44	138.01	0.26	0.52
Significant Damage	333	6.60	2.26	3.04	15.43	13.85	61.54	78.84	0.52	0.26
	1726	6.30	2.16	2.64	13.01	13.24	86.24	96.86	0.66	0.52
	439	6.70	1.79	1.80	8.83	10.47	30.21	25.14	0.30	0.36
	592	6.00	1.95	2.18	9.71	11.56	47.18	41.83	0.16	0.08
	1254	7.60	1.76	1.56	32.24	34.37	90.24	63.83	0.54	0.38
	1257	7.60	2.90	2.39	32.15	33.46	146.44	138.01	0.26	0.52
	591	5.70	3.38	2.56	5.28	5.42	68.80	53.33	0.18	0.34
Near Collapse	42	5.80	5.15	2.50	5.00	4.85	130.69	95.72	0.50	0.25
	7329	6.10	4.12	3.75	4.96	5.52	133.96	108.51	0.46	0.38
	879	6.40	2.67	3.13	16.81	15.54	157.53	187.01	0.34	0.30
	1226	7.60	3.04	3.54	11.81	11.12	108.48	125.88	0.38	0.28
	1560	7.20	7.31	7.85	9.14	8.55	369.53	231.79	0.32	0.36
	5653	5.70	4.34	3.97	2.63	2.40	84.87	75.76	0.12	0.10

7.4.2 TIME-HISTORY ANALYSES OF THE RC FRAME WITH EXTERNAL EXPOSURE (LIMITED DAMAGE – DL)

The results for the most realistic case of the RC structure with external members exposed to different levels of corrosion is herein further investigated. Natural Ground-motions for the limit state DL were used to perform non-linear dynamic analyses. Nonlinear dynamic analyses of the model have been performed for the seven records. The comparison of the mean-relative top displacements versus the corrosion rate obtained from the numerical simulations can be seen in Figures 36. The mean-maximum top displacements were computed in both directions, x and y, from the Nonlinear Static analyses for all the corrosion rates, which was used as an upper bound to check if pushover analyses were able to provide a reliable maximum displacement for the nonlinear dynamic analyses after which the structure fails. Results clearly showed a different behaviour due to diverse level and impact of corrosion on the existing building. The top displacement for each earthquake event increased with a corrosion rate of 5% (an increment of more than 35%) as the RC structure was still able to resist despite the corrosion attack without collapsing, while corrosion level greater than 10% (an increment of more than 25% at CR=10%) caused large and extensive damage to the building. As a result, the building was unable to withstand large displacement and failed earlier than the uncorroded case. Moreover, Figure 23 shows that the maximum displacement from the Nonlinear Static analyses can be used as an upper bound to predict with excellent accuracy the failure of the structure when an event occurs, and the structure is exposed to different levels of corrosion.

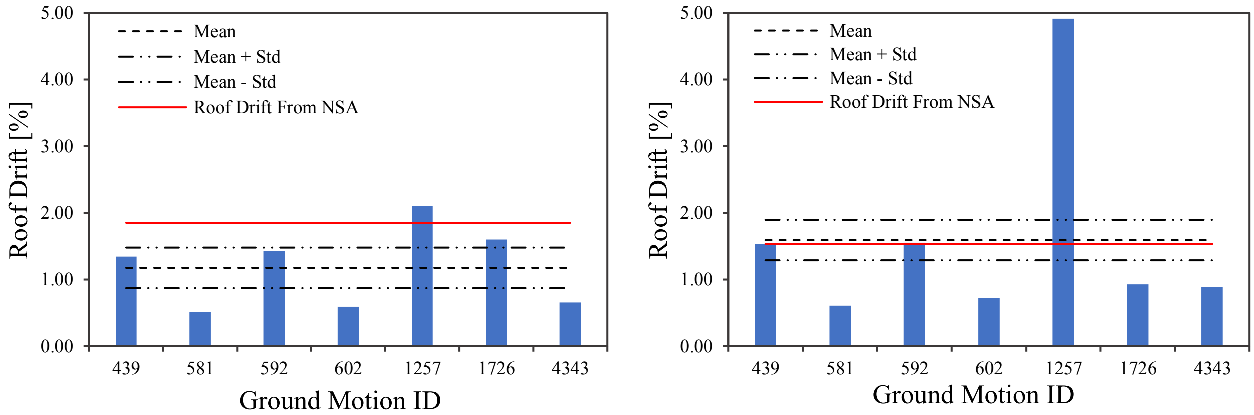

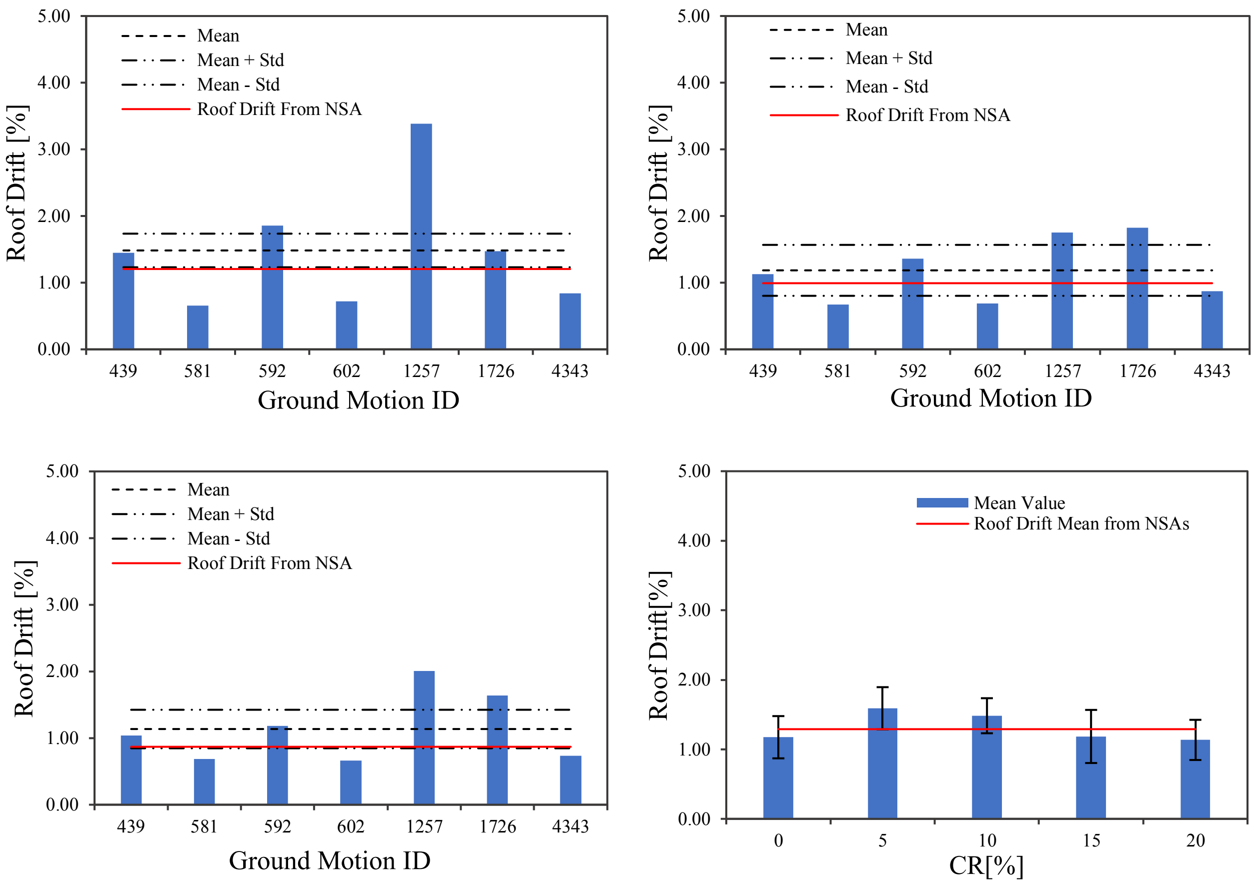

Figure 23. Relative Top Displacement vs Corrosion Rate. a) CR [%] =0; b) CR [%] =5; c) CR [%] = 10; d) CR [%] = 15; e) CR [%] = 20; f) Mean Values

Inter-storey drift is a relevant parameter in terms of structural response as it is related to the damage sustained by buildings during earthquakes and its distribution along the building height can be very useful also to identify soft-storey mechanisms (Elshanai and Di Sarno, 2008). Figures 24 show the drift profiles at the peak displacement for each floor from the numerical time-histories; it is evident that the relative displacement goes up with the increase of the corrosion rate and, particularly, the first and the second floor suffered a large increase in the mean displacement with a corrosion level between 5% and 10, while the third floor slightly increased until the 20% of corrosion. The corrosion attack causes a dramatic increase in the inter-storey drift ratio for the second and the third floors from 1.06% to 2.16% and from 0.93% to 2.02%, respectively. Despite the increase in the corrosion penetration, the relative displacement for rates ranging from 15% to 20% seems to be decreasing, but this is due to the failure of the structure before the earthquake event is complete. Corrosion weakens the structure even if the attack is localized on some members, increasing the inter-storey drift and forcing the structure to collapse earlier for a high level of corrosion.

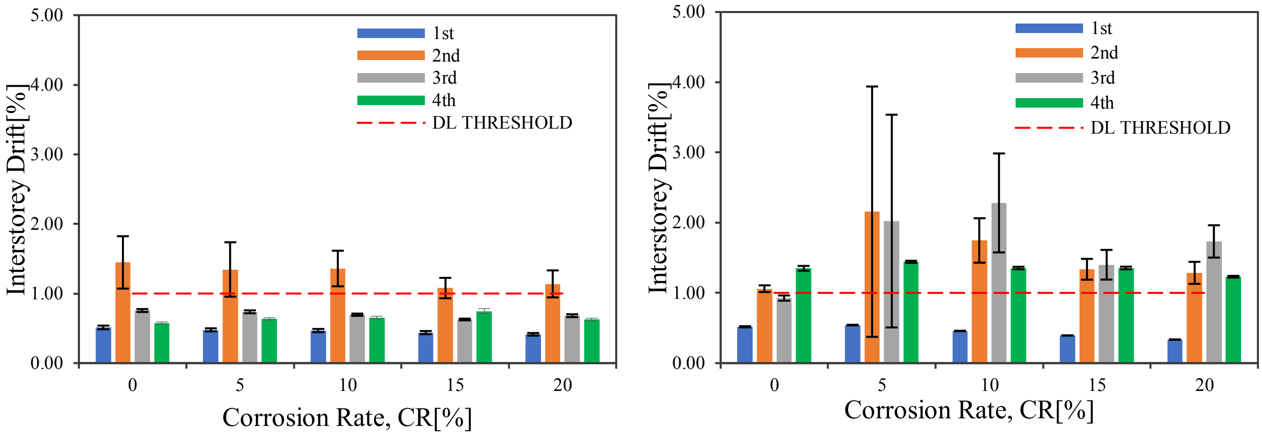

Figure 24. Inter-storey Drift vs Corrosion Rate. a) X-Axis; b) Y-Axis; c) Combination

In order to represent an effective stress-state of the existing building, i.e. a state of deformation that is directly related to the earthquake event, the maximum base shear versus the corrosion rate is provided. Again, a combination of the base shear is given using the following relationship:

$$V_{base,tot} = \sqrt{V_{base,x}^2 + V_{base,y}^2} \tag{20}$$

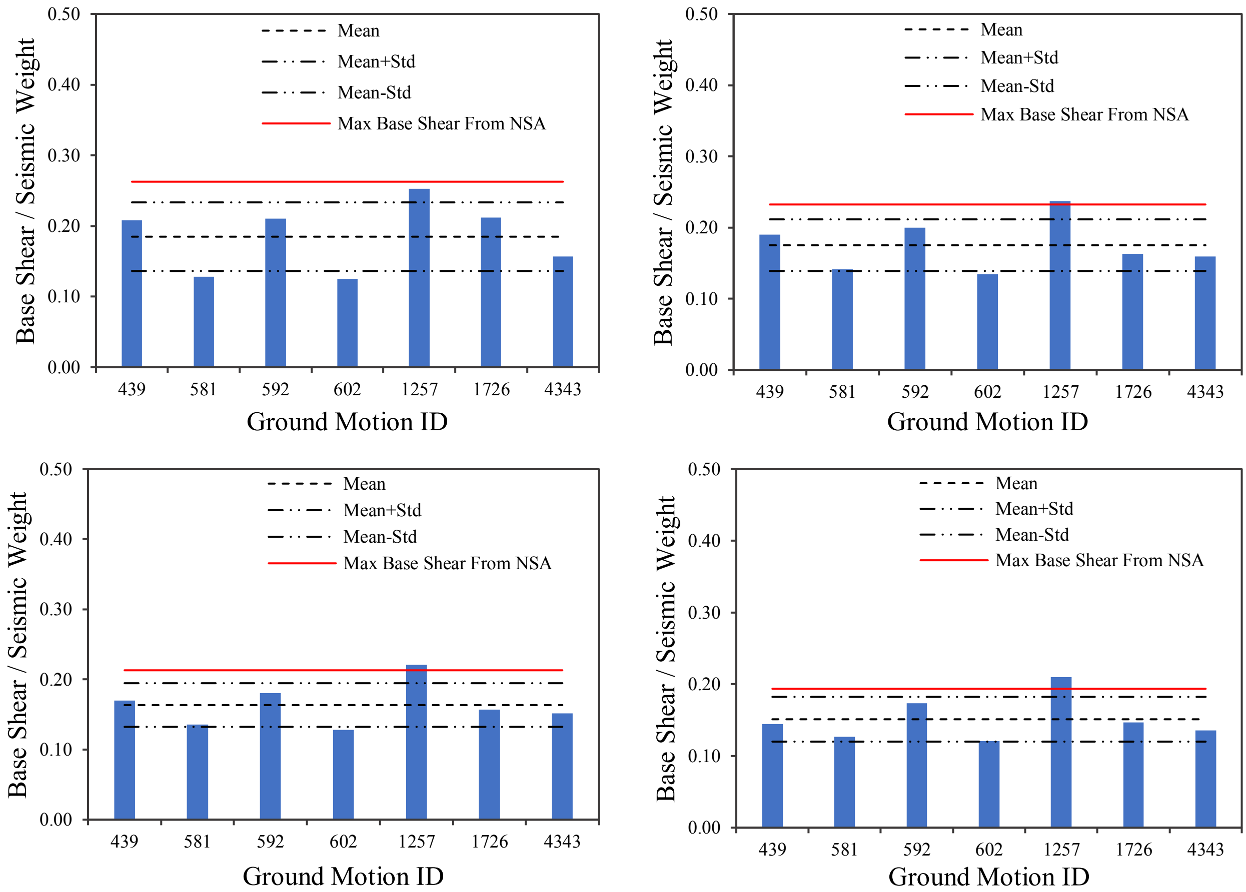

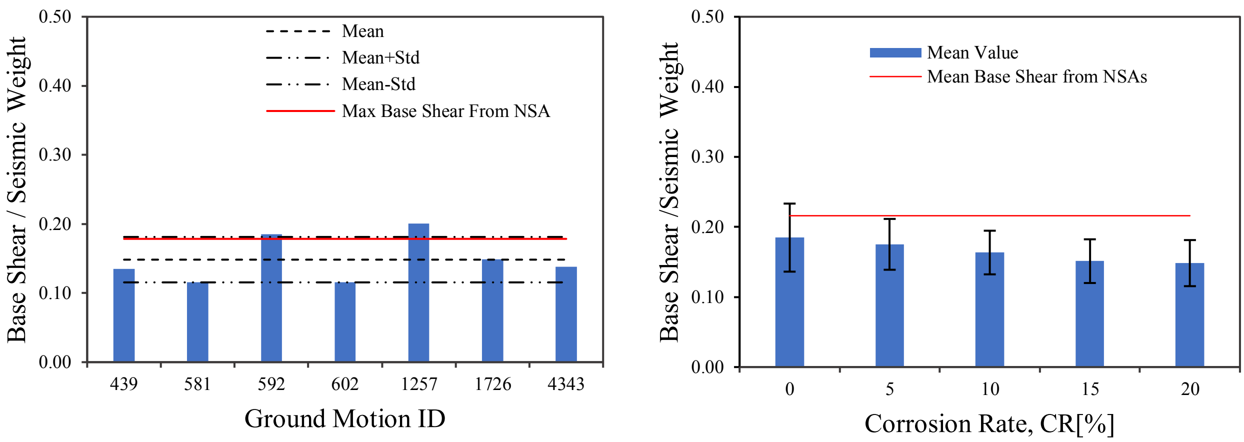

Figure 25. Maximum Base Shear vs Corrosion Rate. a) CR [%] =0; b) CR [%] =5; c) CR [%] = 10; d) CR [%] = 15; e) CR [%] = 20; f) General Plot

Figure 25 clearly showed that the increase in the corrosion rate reduced the maximum base shear of the existing building up to 20%, which demonstrates that the structure is not more able to dissipate the earthquake energy effectively and resist large damage for the same event. The last finding is due mainly to the reduction of the material properties of both the concrete and steel reinforcement, which change the global behaviour of the existing building, in terms of ductility and strength, when exposed to the highly corrosive environment. In addition to this, Figures 25 shows the comparison between the maximum base shear calculated as an average from the nonlinear static analyses using all three lateral loading patterns with those computed from the nonlinear dynamic analyses. Results illustrated that the Pushover analyses overestimate the maximum base shear of the existing building compared to those obtained from the nonlinear dynamic analyses using the seven ground motions for the limit state DL.

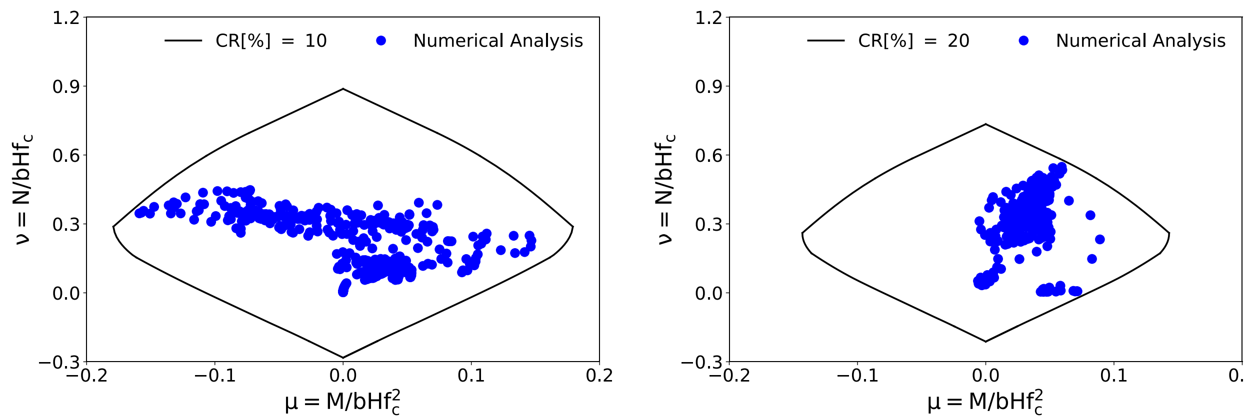

Figure 26. Interaction Surface M-N for the ground motions ID=1726

Within the analyses, each RC member that caused the failure of the building was analysed using the proposed method based on the above-mentioned modified Interaction domain M-N and the pairs M-N computed from the nonlinear dynamic analyses. Some results are shown in Figure 26. Clearly, the outcomes show that the novel approach proposed for the interaction surface of the pair M-N accounting for corrosion is able to predict the failure of RC members, either beam or columns, which caused the collapse of the structure.

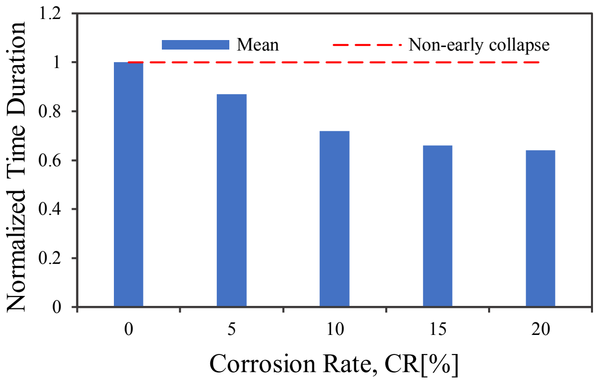

Figure 27. Mean Collapse vs Corrosion Rate

Figure 27 depicts the mean value of the structure failure versus the corrosion rate. The results show that the increase in the corrosion penetration reduces the time of the structural failure, which was mainly due to the external RC members subjected to corrosion.

7.4.3 TIME-HISTORY ANALYSES OF THE RC CONCRETE WITH EXTERNAL EXPOSURE (SIGNIFICANT DAMAGE – SD)

Non-linear dynamic analyses were herein performed to evaluate the seismic response of the corroded existing structure to a selection of seven ground motions for the limit state SD. The results of the nonlinear time-history analyses were assessed considering the mean values and the standard deviations for all the parameters previously mentioned.

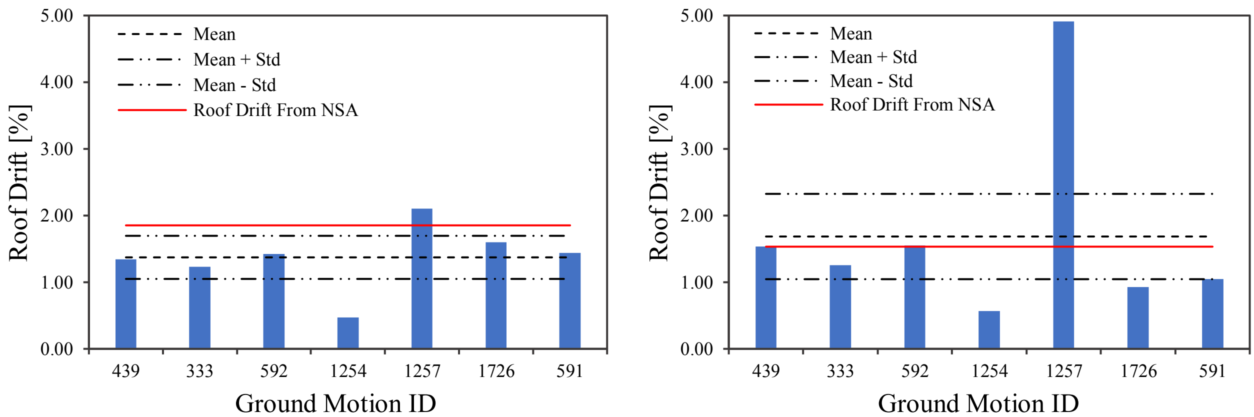

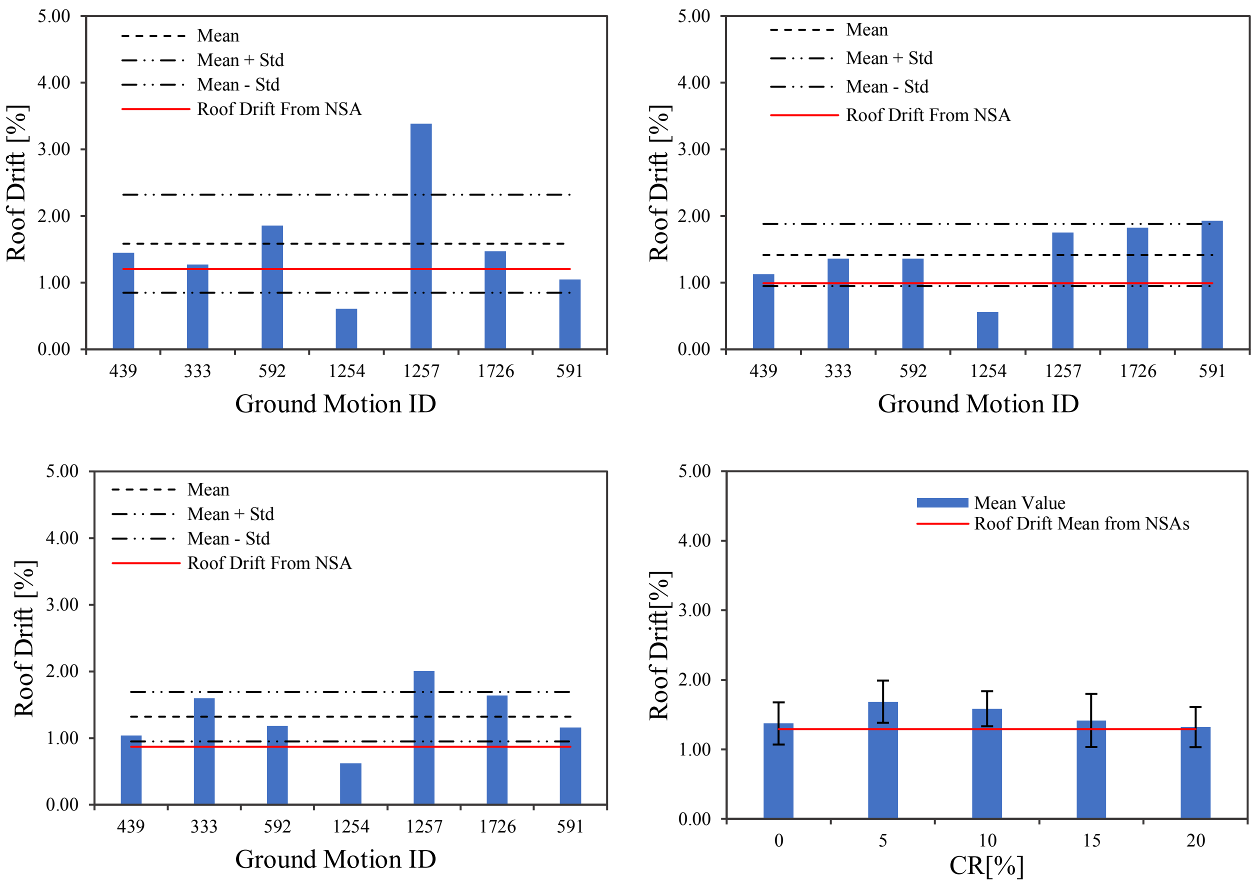

Figure 28. Relative Top Displacement vs Corrosion Rate. a) CR [%] =0; b) CR [%] =5; c) CR [%] = 10; d) CR [%] = 15; e) CR [%] = 20; f) General Plot

Figure 28 depicts the top-drift versus the corrosion rate for all the ground motions. Results show how the impact of corrosion increased the top-drift ratio when the structure was subjected to low levels of corrosion (an increment of more than 22%), which demonstrates that the building was still able to resist extensive damage, while a slight fluctuation can be noted for high levels of corrosion ranging from 10% to 20%. The top-ground drift ratio showed a decreasing variation from 15% to 0% for corrosion levels of 10%-to-20%. Furthermore, the maximum top displacement from the non-linear static analyses was explicitly used as an upper bound to provide a relevant indication of the structural collapse. This parameter clearly decreased with the increase of the corrosion rate, but it could effectively predict the early collapse of the building. As a result, all the top-displacements from nonlinear dynamic analyses greater than the upper bound level from the nonlinear static analyses showed that the corroded building could not dissipate the earthquake energy and collapsed before the earthquake event was complete. An additional plot with the mean and standard deviation to summarize the top-ground drift ratio for all the ground motion is given in Figure 28d.

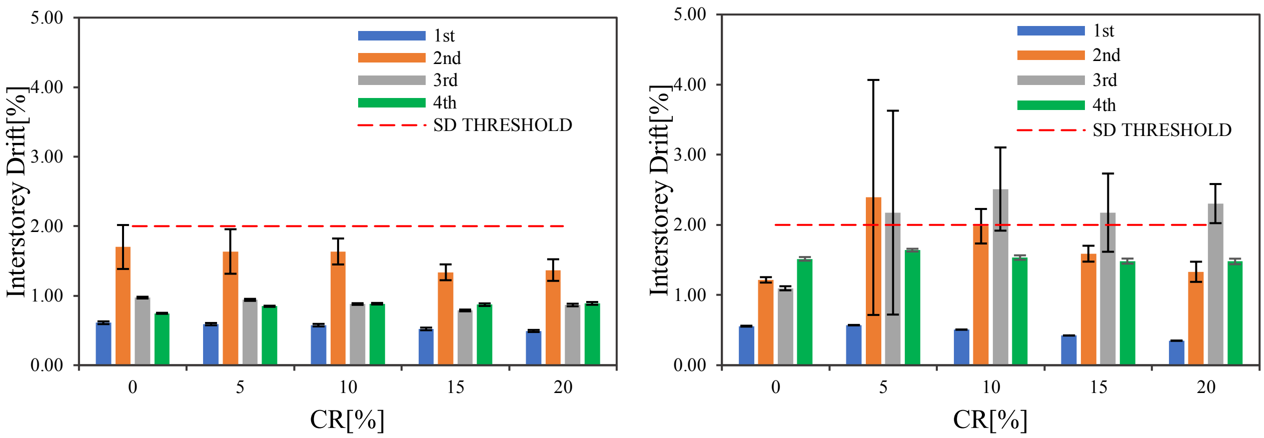

Figure 29. Inter-storey Drift vs Corrosion Rate.

Figure 29 shows the impact of corrosion on the maximum inter-storey-displacement. Results from nonlinear dynamic analyses definitely showed a dramatic increase of the mean lateral inter-storey displacements, and, particularly, the second and the third floors were exposed to large drift-ratios for low levels of corrosion, more than 85% in comparison with the uncorroded case, while a slight variation can be noted for the corrosion rates between 10% and 20%. Again, the slight reduction of the lateral inter-storey displacement for high levels of corrosion in comparison with low levels of corrosion is because the building could not resist large degradation and failure happened before the completion of the earthquake event. In addition, corrosion does not allow the building to comply with the seismic performance imposed by the Eurocode and provisions for the limit state SD. Indeed, the inter-storey lateral displacements were greater than the inter-storey drift limit of 2%, which demonstrates the limits imposed by the technical codes are no longer conservative when RC structures are exposed to highly-aggressive environments. The state of deformation is adequately represented by the variation of the maximum base shear with the increase of the corrosion percentage by using the relationship (20). The combination of the uniform and localized corrosion significantly affects the shear capacity of corroded RC structures, as it can be seen in Figures 30 whereas the maximum base shear is decreasing up to 22% with the increase of the corrosion attack. In addition to the maximum base shear from the nonlinear dynamic analyses, the ultimate shear from the pushover analyses was also provided in Figures 30, which is computed as an average from all the lateral loading patterns in both directions, x and y, and combined using the relationship (20). It should be noted that the pushover analyses overestimated the maximum shear capacity of the corroded building in comparison with the results obtained from the nonlinear dynamic analyses. Only for high levels of the corrosion rate, the mean values of the base shear from nonlinear static analyses could approach those obtained from the nonlinear dynamic analyses.

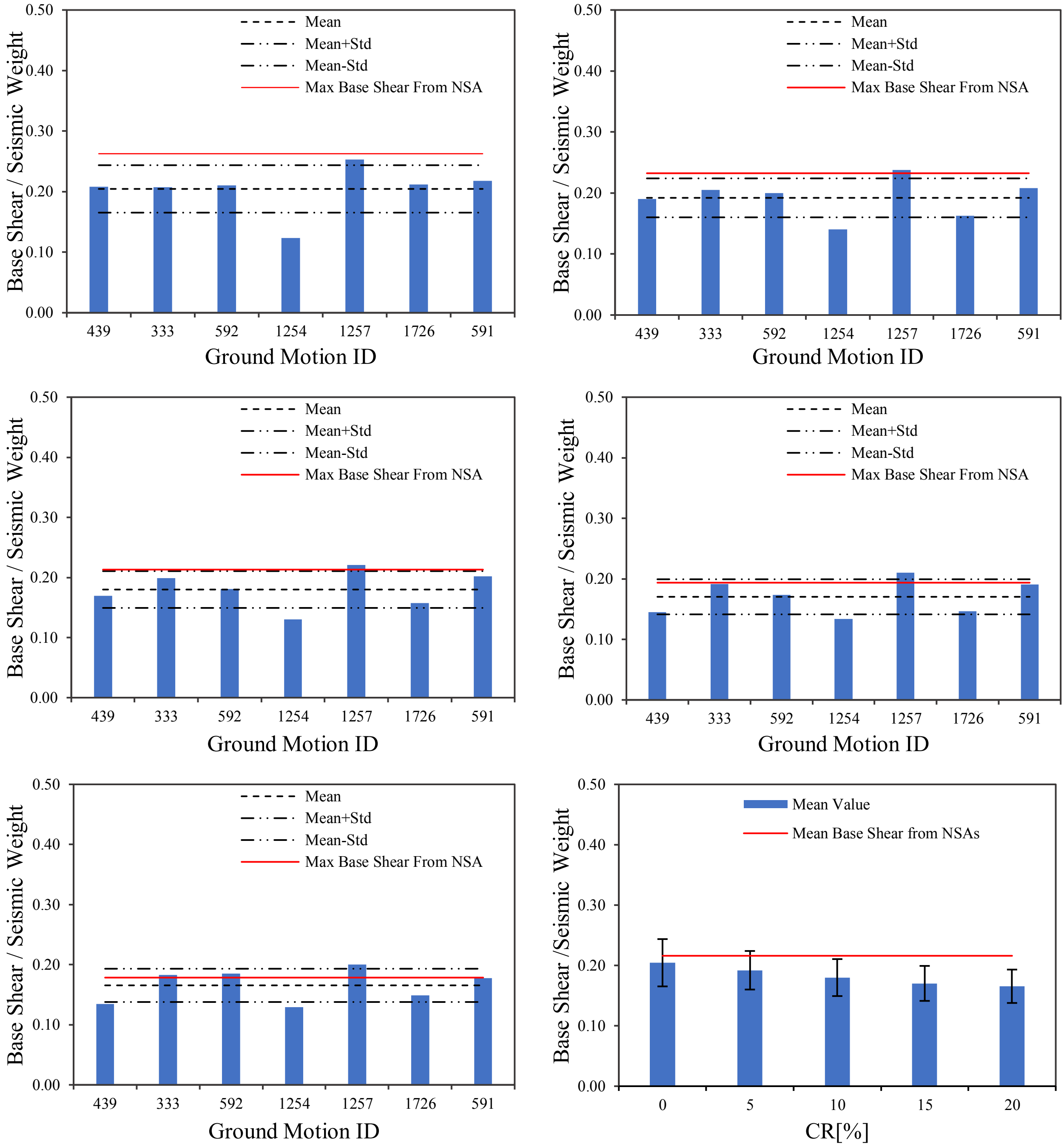

Figure 30. Maximum Base Shear vs Corrosion Rate. a) CR [%] =0; b) CR [%] =5; c) CR [%] = 10; d) CR [%] = 15; e) CR [%] = 20; f) General Plot

Figure 31 illustrates the mean-collapse duration-time versus the corrosion rate. Results show that the dramatic decay of the concrete and steel's mechanical properties, as well as the loss of the global shear strength, force the structure to collapse before the duration of the earthquake. Furthermore, because of the greater peak ground accelerations for the limit state SD, the structure exhibits even lesser resistance, in comparison with the limited damage, to an earthquake event as the corrosion rate goes up.

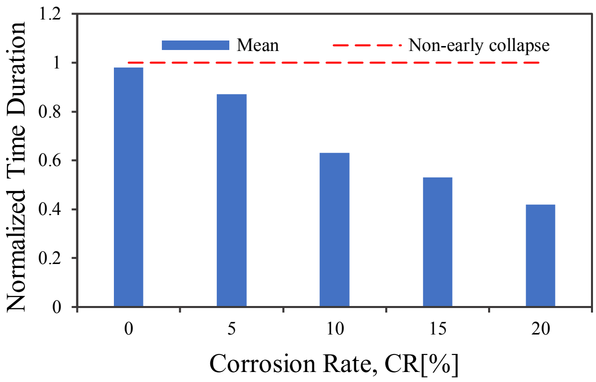

Figure 31. Mean Collapse vs Corrosion Rate

During the analyses, the RC components which induced the collapse of the structure were picked and checked against the proposed modified interaction surface M-N for corroded RC. Figure 32 shows the interaction surfaces of the pair M-N computed for the critical RC components. The outcomes show that the proposed method could predict with excellent accuracy the ultimate resistance of a corroded RC element, either beam or column.

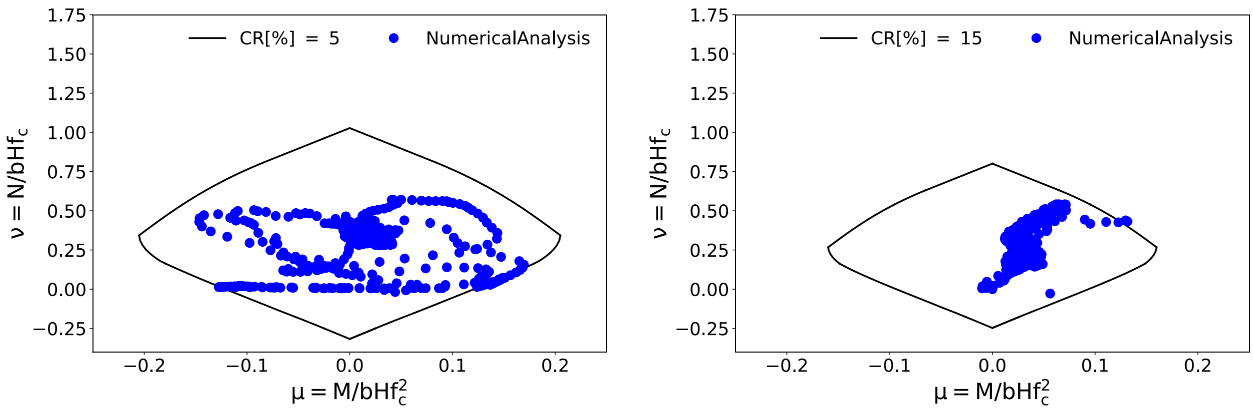

Figure 32. Interaction Surface M-N for the ground motion ID = 591

7.4.4 TIME-HISTORY ANALYSES OF THE RC CONCRETE WITH EXTERNAL EXPOSURE (NEAR COLLAPSE – NC)

The seismic performance of the existing RC building with the external exposure is here investigated for the limit state NC.

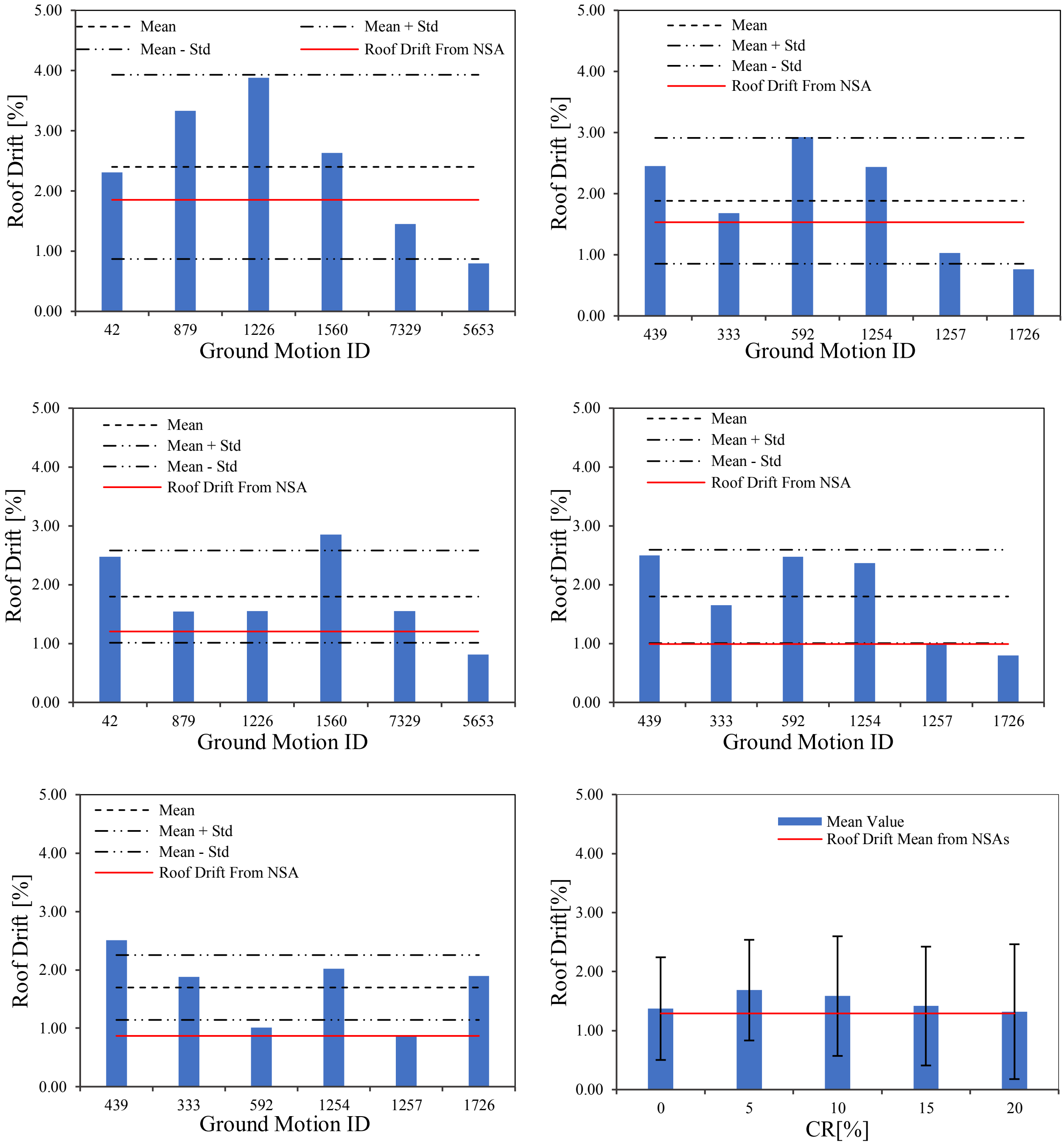

Figure 33. Relative Top Displacement vs Corrosion Rate. A) CR [%] =0; b) CR [%] =5; c) CR [%] = 10; d) CR [%] = 15; e) CR [%] = 20; f) General Plot

Figure 33 demonstrated that the top-ground drift ratio decreased significantly with the increase of the corrosion rate due to the early collapse of the structure, which was already not able to resist large earthquakes, even if uncorroded. The last observations can be found in the lack of the seismic details and, particularly, due to i.e. small stirrups spacing and diameter. The reduction of the top displacement entails that the corrosion attack lowers the mechanical properties of the concrete and the steel reinforcement such that even a corrosion rate of 5% forced the structure to fail before the completion of the earthquake event. The displacement of the control node from the nonlinear static analyses was also depicted for all corrosion levels. The results show that, despite the displacements from the pushover analyses were smaller than the mean values computed for the nonlinear dynamic analyses, they were handful parameters to detect the maximum value beyond which the structure would fail. Figure 33d summarizes the outcomes for the top-ground drift ratio from the nonlinear time-history analyses in terms of mean drift ratio and standard deviation.

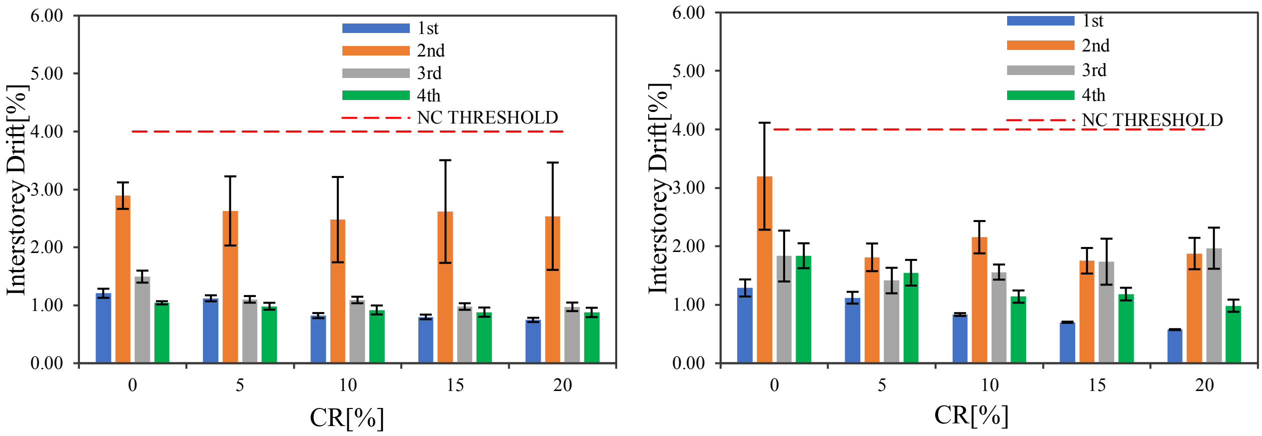

Figure 34. Inter-storey Drift vs Corrosion Rate.

Figure 34 illustrates the results for the inter-storey drift ratio versus the corrosion rate. The outcomes clearly demonstrated that the structure with low and high levels of corrosion could not withstand extensive damage and deterioration, so large inter-storey displacement can be noted for the second floor even when the building is uncorroded. A relevant decrease (almost 23%) in the inter-storey displacement can be seen in Figure 34 as the corrosion level went up. Furthermore, it should be noticed that the maximum inter-storey drift defined by the Eurocode (EN 1998-1 (2004) and provisions (FEMA 356, 2000) is no longer conservative when corrosion occurs as the structure failed before reaching the allowable limit of 4% for the limit state NC.

The maximum base shear for all the corrosion scenarios is also given in Figures 35. The outcomes showed that the impact of corrosion affects significantly the shear capacity of the structure, which dramatically decreased up to 27% with the increase of the corrosion penetration. Moreover, the maximum base shear from the pushover analyses was also provided to compare the results between the nonlinear static and dynamic analyses. The values of the maximum base shear from the pushover analyses seem to underestimate the shear capacity of the corroded building for the limit state of NC. They are always smaller than the mean values obtained from the nonlinear dynamic analyses. Additionally, to evaluate the impact of corrosion in terms of collapse time, Figure 50 shows the mean collapse duration versus the corrosion level. The results clearly demonstrated that the time of failure reduced with the increase of the corrosion level even when the 1053 structure was uncorroded, which entails that the building could not resist the selection of real1054 ground motion for the limit state of

Near Collapse. Finally, the RC elements that caused the structural collapse were picked during the analyses and verified against the proposed modified interaction surface of the pair M-N. Figures 49 show that the suggested method can predict with accuracy the ultimate capacity of RC components responsible for the structural failure.

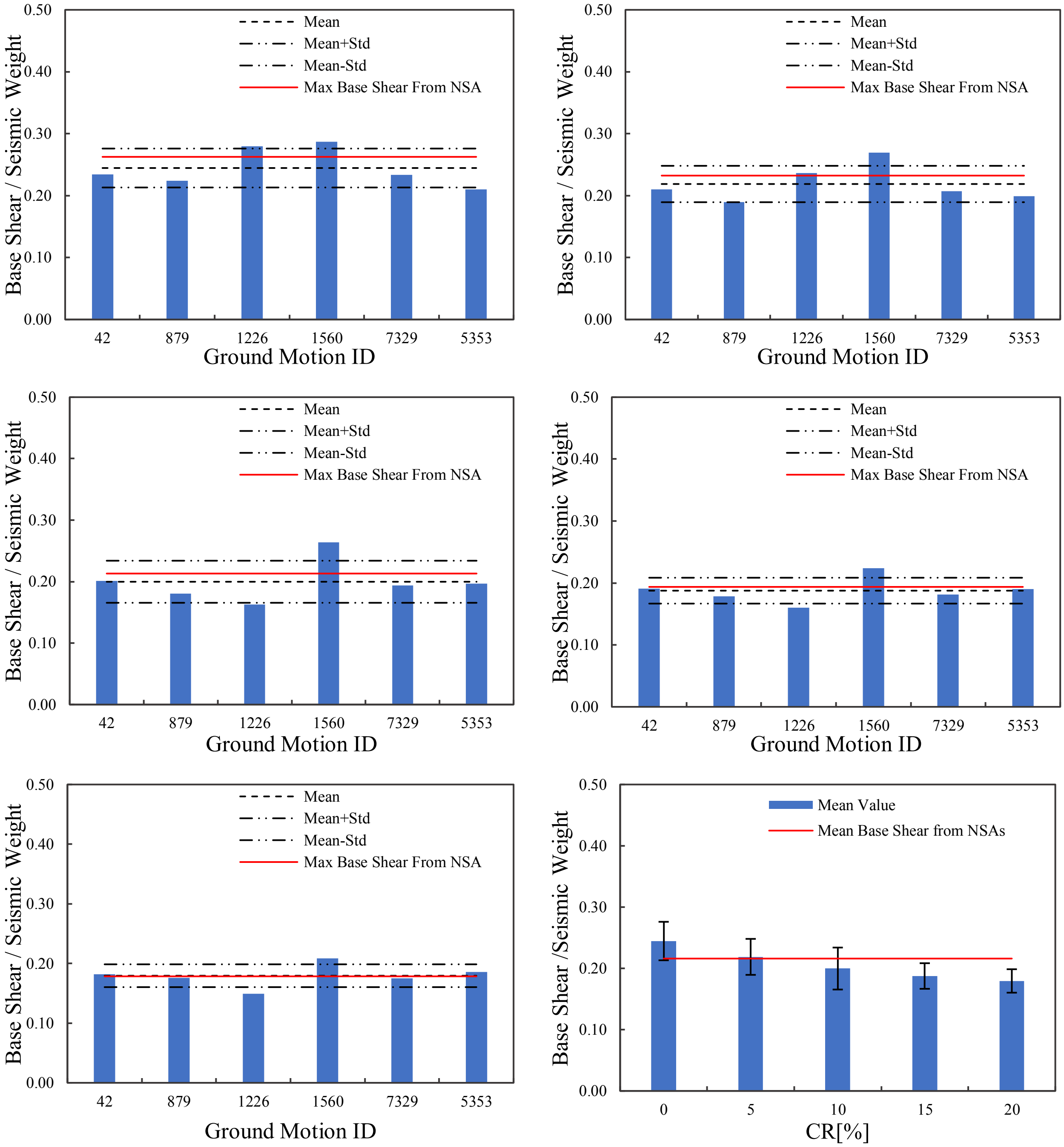

Figure 35. Maximum Base Shear vs Corrosion Rate. a) CR [%] =0; b) CR [%] =5; c) CR [%] = 10; d) CR [%] = 15; e) CR [%] = 20; f) General Plot

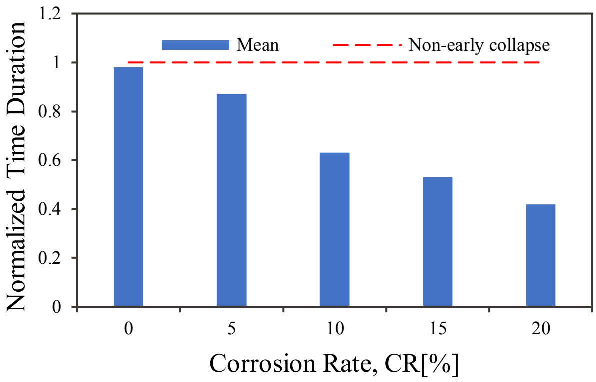

Figure 366. Mean Collapse vs Corrosion Rate

Figure 36 shows the mean collapse duration versus the corrosion level. The results clearly demonstrated that the time of failure reduced with the increase of the corrosion level even when the structure was uncorroded, which entails that the building could not resist the selection of real-ground motion for the limit state of Near Collapse.

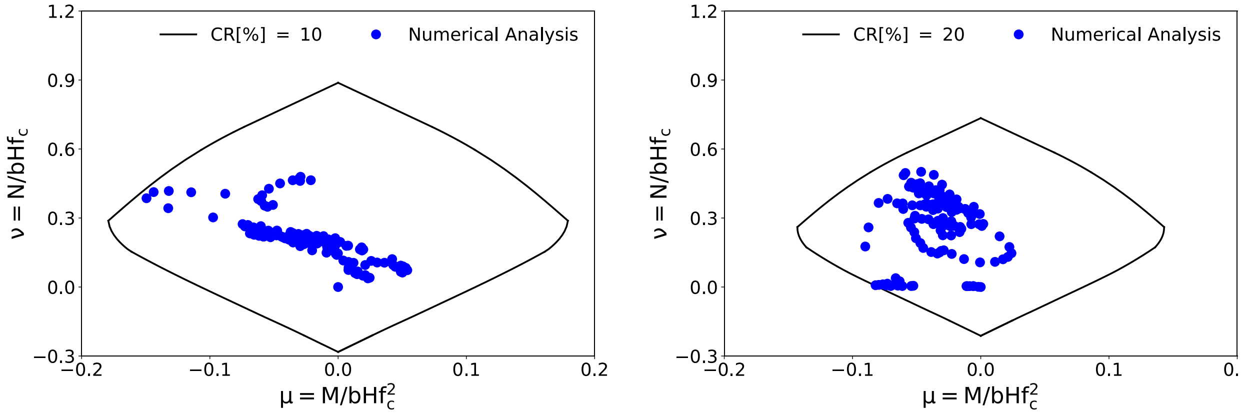

Figure 37. Interaction Surface M-N for the ground motion ID = 879

Finally, the RC elements that caused the structural collapse were picked during the analyses and verified against the proposed modified-interaction surface of the pair M-N. Figures 49 show that the suggested method can predict with accuracy the ultimate capacity of RC components responsible for the structural failure.

8 CONCLUSIONS

The interest for the RC structures exposed to corrosion has increased in the scientific community over the last years as many studies have been conducted on the experimental and numerical response of corroded RC elements. This topic remains an open issue for the many uncertainties related to the corrosion phenomenon, and, therefore, such investigation is a significant step forward to establish new inspection-ratings and preserve the safety of aged RC buildings. This study presents a numerical investigation of the seismic performance of typical reinforced concrete buildings with smooth rebars exposed to different levels of corrosion. A numerical approach has been proposed to evaluate the ultimate capacity of RC members and corroded RC columns under static and dynamic loadings. The results obtained from the numerical investigations can be summarized as follows:

- The proposed numerical method can predict with excellent accuracy the ultimate capacity of corroded RC components with various reinforcement ratios, i.e. 0.5%, 2.01% and 2.26%. under static and dynamic loading condition.
- Non-linear static analyses based on four different exposure and three lateral loading patterns demonstrated that corrosion significantly reduces the shear capacity and the global ductility of an existing RC building. Particularly, the shear strength reduction ranged between 20%, for the external exposure, and 50%, for the entire structure exposed to corrosion. In addition, corrosion forced the structure to move from a ductile to a brittle failure mechanism.
- Ductility and overstrength were strongly affected by the impact of corrosion. Particularly, results showed that these two parameters had different trends depending on the type of exposure and the choice of some factors such as yielding force, yielding displacement, ultimate force and ultimate displacement. The exposure of the total structure to corrosion appeared to be the worst scenario with a decrease of both parameters by more than 30%.
- Performance indicators evaluated in the present study could be successfully used to assess the seismic performance of the corroded RC building. These performance points would be beneficial to design a new strategy for retrofitting deteriorated RC structures.
- The results from Non-linear dynamic analyses, considering only the external exposure, showed that the impact of corrosion strongly affects the strength, the deformability, the ductility and the energy absorption of an existing corroded RC building during a seismic event. A consistent reduction of the maximum base shear, and a significant increase of the top-ground and inter-storey drift ratios was observed. In addition, the increase of the axial loads and bending levels were also an indication of the catastrophic response of corroded RC elements during seismic events, which was well-evaluated via the use of the proposed interaction surface of the pair M-N.
- Comparison between the nonlinear static and dynamic analyses demonstrated that the displacements from the pushover analyses could be used as an upper bound to evaluate the point beyond which the structure will fail during a real seismic event. By contrast, it is worth noting that nonlinear static analyses overestimated the shear strength for the limit state of the

Limited Damage and Significant Damage, while underestimated it for the limit state of the Near Collapse, compared to non-linear dynamic analyses.

9 ACKNOWLEDGEMENTS

The authors would like to gratefully acknowledge the financial support of this work through the EPSRC and ESRC Centre for Doctoral Training in Quantification and Management of Risk and Uncertainty in Complex Systems Environments Grant No. (EP/L015927/1).

10 REFERENCES

1. Andisheh K., Scott A. and Palermo A., Seismic Behavior of Corroded RC Bridges: Review and Research Gaps, *International Journal of Corrosion*, vol. 2016, Article ID 3075184, 22 pages, 2016. https://doi.org/10.1155/2016/3075184.

2. Andrade, C., Alonso, C., Garcia, F and Rodriguez, J. (1991), Remaining Lifetime of Reinforced Concrete Structures: Effect of Corrosion in the Mechanical Properties of the Steel, Life Prediction of Corrodible Structures, NACE, Cambridge, UK; pg. 12/1-12/11

3. Angst, U.M. (2018). Challenges and opportunities in corrosion of steel in concrete. *Materials and Structures* 51: 4. https://doi.org/10.1617/s11527-017-1131-6.

4. Azad, A. K., Ahmad, S., and Al-Gohi, B. (2010). Flexural strength of corroded reinforced concrete beams. *Mag. Concr. Res.*, 62(6),405–414.

5. Bertolini L., Carsana M., Gastaldi M., Lollini F. and Redaelli E. (2016). Corrosion of Steel in Concrete and Its Prevention in Aggressive Chloride-Bearing Environments. *5th International Conference on Durability of Concrete Structures* Jun 30–Jul 1, 2016, Shenzhen University, Shenzhen, Guangdong Province, China

6. Bhide, S. (1999), Material Usage and Condition of Existing Bridges in the {U.S.}. *Skokie, Ill.*

7. Biondini F., Camnasio E. & Palermo A. (2014) Lifetime seismic performance of concrete bridges exposed to corrosion, *Structure and Infrastructure Engineering*, 10:7, 880-900, DOI: 10.1080/15732479.2012.761248

8. Biondini F., Palermo A. and Toniolo G. (2011), Seismic performance of concrete structures exposed to corrosion: case studies of low-rise precast buildings, *Structure and Infrastructure Engineering* Vol. 7, Nos. 1–2, 109–11

9. Biskinis DE, Fardis MN (2007) Effect of lap splices on flexural resistance and cyclic deformation capacity of members. *Beton- und Stahlbetonbau, Sonderheft Englisch* 102: 51–59

10. Biskinis DE, Fardis MN (2009) Upgrading of resistance and cyclic deformation capacity of deficient concrete columns. In: Ilki A et al. (ed) Seismic Risk Assessment and Retrofitting, with Special Emphasis on Existing Low-Rise Structures, *Springer Verlag, Heidelberg*

11. Cairns, J., Plizzari, G., Du,Y. Law, D.W. and Franzoni C., (2005), Mechanical Properties of Corrosion-Damaged Reinforcement, *ACI Materials Journal*, Vol. 102 n°4, pg. 256-264

12. Celarec, D., Vamvatsikos, D. & Dolšek, M. (2011). Simplified estimation of seismic risk for reinforced concrete buildings with consideration of corrosion over time. *Bulletin of Earthquake Engineering* (2011) 9: 1137. https://doi.org/10.1007/s10518-010-9241-3.

13. Claisse, P.A. (2008) Corrosion of steel in concrete – understanding, investigation and repair 2nd edn. Broomfield J. P., Taylor & Francis, London, 2006., 978-0-4153-3404-4, p. 296. *Proceedings of the ICE - Construction Materials*, volume 161 (3): 135.

14. Clark, L. A. and Saifullah, M. (1994), Effect of Corrosion Rate on the Bond Strength of Corroded Reinforcement, *Corrosion and Corrosion Protection of Steel in Concrete*, R.N. Swamy, Sheffield Academic Press, pg. 591-602

15. Coronelli and Gambarova (2004), Structural Assessment of Corroded Reinforced Concrete Beams: Modeling Guidelines, ASCE J. of Structural Engineering VOL 130 Issue 8

16. Di Sarno L. and Pugliese F. (2019), Critical review of models for the assessment of the degradation of reinforced concrete structures exposed to corrosion, *Conference SECED 2019, Earthquake Risk and Engineering towards a Resilient World*

17. Du Y., L. A. Clark L. A. and Chan, A. H. C. (2005). Residual capacity of corroded reinforcing bars. Magazine of Concrete Research, 2005, 57, No. 3, April, 135–147

18. Du, Y (2001). Effect of Reinforcement Corrosion on Structural Concrete Ductility, *PhD Thesis*, University of Birmingham, UK, 320 pg.

19. Elnashai, A. S., & Di Sarno L. (2008). Fundamentals of Earthquake Engineering. *John Wiley and Sons*. http://doi.org/10.1002/9780470024867.

20. Emilio Bastidas-Arteaga (2018). Reliability of Reinforced Concrete Structures Subjected to Corrosion-Fatigue and Climate Change. *International Journal of Concrete Structures and Materials*, Springer, 2018, 12(1), 10.1186/s40069-018-0235-x. hal-01698136

21. EN 1992-1-1 Eurocode 2: Design of concrete structures - Part 1-1: General rules and rules for buildings E. for Standardization. *Brussels, EN, CEN, (2005)*

22. EN 1998-1 (2004). Eurocode 8: Design of Structures for Earthquake Resistance. Part - 3. *1st ed. Brussels: BSi*

23. Fardis, M (2009). Seismic Design, Assessment and Retrofitting of Concrete Buildings. *Springer Netherlands*, XXIV, 744, ISBN: 978-1-4020-9842-0. DOI: 10.1007/978-1-4020-9842-0.

24. Fardis, M.N. and Calvi, M.C. (1994). Effects of infills on the global response o reinforced concrete frames," *Proceedings of the 10th European Conference on Earthquake Engineering*, A.A. Balkema, Rotterdam, Vol. 4, pp. 2893-2898.

25. FEMA 356 (2000). Prestandard and Commentary for the Seismic Rehabilitation of Buildings. *Washington DC*.

26. H. S., Tomosawa, F. and Noguchi, T. (1996), Effect of Rebar Corrosion on the Structural Performance of Singly Reinforced Beams, *Durability of Building Materials and Components*, Vol. 7, C. Sjostrom, E&FN Spon, London, pg. 571-580

27. Hailong Ye, Chuanqing Fu, Nanguo Jin, Xianyu Jin, (2018). Performance of reinforced concrete beams corroded under sustained service loads: A comparative study of two accelerated corrosion techniques. *Construction and Building Materials* 162, pag. 286-297

28. Hakan Yalciner, Serhan Sensoy, and Ozgur Eren (2015), Seismic Performance Assessment of a Corroded 50-Year-Old Reinforced Concrete Building, *American Society of Civil Engineers*

29. Imperatore, S., Rinaldi, Z. and Drago C. (2017), Degradation Relationships for the Mechanical Properties of Corroded Steel Rebars, *Construction and Building Materials*, Vol. 148, pg. 219-230

30. Inamullah Khan, Raoul François, Arnaud Castel. (2014). Experimental and analytical study of corroded shear-critical reinforced concrete beams, *Materials & Structures*, Volume 47, Issue 9 (2014), Page 1467-1481, DOI 10.1617/s11527-013-0129-y, 2014

31. J. Cairns, Y. Du and D. Law (2008). Structural performance of corrosion-damaged concrete beams. *Magazine of Concrete Research*, 2008, 60, No. 5, June, 359–370 DOI: 10.1680/macr.2007.00102.

32. Kappos, A. J. and Ellul, F. (2000). Seismic design and performance assessment of masonry infilled RC frames. In *Proceedings of the 12th world conference on earthquake engineering*, paper (No. 989).

33. Kose M. M. (2009). Parameters Affecting the Fundamental Period of RC Buildings with Infill Walls. *Engineering Structures*, vol. 31, pp. 93-102.

34. Mohsen Ali Shayanfar, Mohammad Ali Barkhordari and Mohammad Ghanooni-Bagha (2016). Effect of longitudinal rebar corrosion on the compressive strength reduction of concrete in reinforced concrete structure. *Advances in Structural Engineering* 2016, Vol. 19(6) 897–907

35. Morinaga, S. (1996), Remaining Life of Reinforced Concrete Structures after Corrosion Cracking, *Durability of Building Materials and Components*, C. Sjostrom, ed., E&FN Spon, London 1996, pp. 127-137

36. Pritzl, M. D., Tabatabai, H., & Ghorbanpoor, A. (2014). Laboratory evaluation of select methods of corrosion. International Journal of Concrete Structures and Materials prevention in reinforced concrete bridges. *International Journal of Concrete Structures and Materials*, 8(3),201–212.https://doi.org/10.1007/s40069-014-0074-3

37. Pugliese F., Di Sarno L. and Mannis A. (2019), Numerical Evaluation of Reinforced Concrete Frames with Corroded Steel Reinforcement under seismic loading. A Case Study, *Conference ICSBS 2019, 2nd International Conference on Sustainable Buildings and Structures*

38. Radlinska, A., McCarthy, L. M., Matzke, J., & Nagel, F. (2014). Synthesis of DOT use of beam end protection for extending the life of bridges. *International Journal of Concrete Structures and Materials*, 8(3), 185–199.https://doi.org/10.1007/s40069-014-0077-0

39. Raoul François, Stéphane Laurens and Fabrice Deby (2018), Corrosion and its Consequences for Reinforced Concrete Structures, *ISTE Press - Elsevier*, 232 pages, ISBN 978-1-78548-234-2

40. Rodriguez, J., Ortega, L. M., and Casal, J. (1997). Load carrying capacity of concrete structures with corroded reinforcement. *Construction Building Materials*,1(4), 239–248.

41. S.T. Karapetrou, S.D. Fotopoulou, K.D. Pitilakis, (2017). Seismic Vulnerability of RC Buildings under the Effect of Aging. *Procedia Environmental Sciences*, Volume 38, 2017, Pages 461-468, ISSN 1878-0296, https://doi.org/10.1016/j.proenv.2017.03.137.

42. Seismosoft (2018). SeismoStruct - A computer program for static and dynamic nonlinear analysis of framed structures; *URL: https://seismosoft.com*.

43. Seismosoft Sample Models (2018). SeismoStruct - A computer program for static and dynamic nonlinear analysis of framed structures. A Case Study; *URL: https://seismosoft.com/seismobuild-seismostruct-sample-models*.

44. Torres-Acosta, A. A., Navarro-Gutierrez, S., and Teran-Guillen, J. (2007). Residual flexure capacity of corroded reinforced concrete beams. *Eng. Struct*., 29(6), 1145–1152 for buildings

45. Tuutti, K. (1982). Corrosion of steel in concrete. *Swedish Cement and Concrete Research Institute, Stockholm.*

46. Val, D., and Chernin, L. (2009). Serviceability reliability of reinforced concrete beams with corroded reinforcement. *J. Struct*. Eng.,10.1061/(ASCE)0733-9445(2009)135:8(896),896–905.

47. Vecchio and Collins (1986). The Modified Compression-Field Theory for Reinforced Concrete Elements Subjected to Shear. ACI Journal 83-22

48. Wang, X. and Liu, X (2008), Modeling the Flexural Carrying Capacity of Corroded RC Beams, *J. Shangai Jiaotong Univ.* (Sci.), 13(2): 129-135

49. Xia, J., Jin, W. L., and Li, L. Y. (2011). Shear performance of reinforced concrete beams with corroded stirrups in chloride environment. *Corros. Sci*., 53(5), 1794–1805.

50. Zandi Hanjari, K., Kettil, P., and Lundgren, K. (2011). Analysis of Mechanical Behavior of corroded Reinforced Concrete Structures. ACI Structural Journal, vol. 108(5), pp. 532-541.

51. Zhang M., Liu R., Li Y. and Zhao G. (2018). Seismic Performance of a Corroded Reinforced Concrete Frame Structure Using Pushover Method, *Advances in Civil Engineering*, vol. 2018, Article ID 7208031, 12 pages, 2018. https://doi.org/10.1155/2018/7208031.

52. Zhang, P. S., Lu, M. and Li, X. (1995), The Mechanical Behaviour of Corroded Bar, *Journal of Industrial Buildings*, Vol. 25, N°257. pg. 41-44